

Department of Chemistry  
Faculty of Science  
University of Helsinki

**COMPUTATIONAL STUDIES ON CHEMICAL IONIZATION  
AND REACTION RATES OF ATMOSPHERICALLY RELEVANT  
OXIDIZED MULTIFUNCTIONAL COMPOUNDS**

**Noora Hyttinen**

ACADEMIC DISSERTATION

To be presented, with the permission of the Faculty of Science of the University of Helsinki, for public examination in Auditorium A129 of the Department of Chemistry (A.I. Virtasen aukio 1, Helsinki) on 24 August 2018, at 12 noon.

Helsinki 2018

<b>Author's address</b>	Department of Chemistry P.O. Box 55 FI-00014 University of Helsinki noora.hyttinen@helsinki.fi
<b>Supervisor</b>	Docent Theo Kurtén, Ph.D. Department of Chemistry University of Helsinki, Finland
<b>Supervising professor and custos</b>	Professor Lauri Halonen, Ph.D. Department of Chemistry University of Helsinki, Finland
<b>Reviewers</b>	Professor Brian Heikes, Ph.D. Graduate School of Oceanography The University of Rhode Island, USA  Assistant Professor Antti Karttunen, Ph.D. Department of Chemistry and Material Science Aalto University, Finland
<b>Opponent</b>	Associate Professor Joseph Lane, Ph.D. School of Science University of Waikato, New Zealand

ISBN 978-951-51-4411-9 (pbk.)  
ISBN 978-951-51-4412-6 (PDF)  
<http://ethesis.helsinki.fi/>

Unigrafia  
Helsinki 2018

## ABSTRACT

High pressure chemical ionization has recently been used with mass spectrometers to measure atmospheric molecules and molecule clusters. In anion chemical ionization, negatively charged reagent ions ionize the neutral sample molecules (or clusters) mainly by forming ion-molecule clusters. The detection of neutral molecules is highly dependent on how effective the chemical ionization processes are, since the mass spectrometers can only detect charged molecules or clusters. This causes uncertainties in the measurements of most atmospheric trace gas molecules. In addition, mass spectrometers are able to detect only the molecular mass of the sample molecules, which means that other methods are needed to find the molecular structures of the detected compounds. In this work, we take a look at how quantum chemistry can be used to model different chemical ionization processes in a typical chemical ionization instrument, and to calculate reaction rates for unimolecular gas-phase reactions.

With our computations, we were able to explain some of the experimental observations regarding the differences in the detection efficiencies of some reagent ions. The cause for the low detection efficiency of some sample molecules was found to be less stable ion-molecule clusters. Our calculations showed an increasing cluster stability for each of the studied reagent anions with the increase of the number of oxygen atoms in the sample molecule. This means that less oxygenated molecules generally have lower detection efficiencies than the more oxygenated ones. In addition, the computed reaction rate coefficients of two different unimolecular HO<sub>2</sub> loss reaction mechanisms showed that, due to collisional stabilization, this reaction is too slow to compete with bimolecular reactions under atmospheric conditions, especially if the reactant is an oxygenated organic molecule.

## ACKNOWLEDGEMENTS

I want to thank my supervisor Docent Theo Kurtén for giving me the opportunity to do my PhD in his group. I also want to thank Professor Lauri Halonen for the chance to work in the Laboratory of Physical Chemistry.

I am grateful to Professor Brian Heikes and Assistant Professor Antti Karttunen for reviewing the thesis and to all of the co-authors for giving excellent feedback.

I am thankful for all past and present members and visitors of the Computational atmospheric chemistry group. I am also thankful for the past and present members of the Computational aerosol physics group for all of the free time activities, and the Kjaergaard group for the educational CopenHel meetings.

The Academy of Finland is acknowledged for funding and CSC-IT Center for Science for computing time. Nordplus and CHEMS are thanked for travel grants.

Noora Hyttinen

Helsinki, 2018

## LIST OF PUBLICATIONS AND AUTHOR'S CONTRIBUTIONS

List of publications included in the thesis:

- I **Noora Hyttinen**, Oona Kupiainen-Määttä, Mikko Muuronen, Matti P. Rissanen, Mikael Ehn, Theo Kurtén. Modeling the charging of highly oxidized ozonolysis products using nitrate-based chemical ionization. *The Journal of Physical Chemistry A* **2015**, *119*, 6339-6345.
- II **Noora Hyttinen**, Matti P. Rissanen, Theo Kurtén. Computational comparison of acetate and nitrate chemical ionization of highly oxidized cyclohexene ozonolysis intermediates and products. *The Journal of Physical Chemistry A* **2017**, *121*, 2172-2179.
- III **Noora Hyttinen**, Rasmus V. Otkjær, Siddharth Iyer, Henrik G. Kjaergaard, Matti P. Rissanen, Paul O. Wennberg, Theo Kurtén. Computational comparison of different reagent ions in the chemical ionization of oxidized multifunctional compounds. *The Journal of Physical Chemistry A* **2018**, *122*, 269-279.
- IV **Noora Hyttinen**, Hasse C. Knap, Matti P. Rissanen, Solvejg Jørgensen, Henrik G. Kjaergaard, Theo Kurtén. Unimolecular HO<sub>2</sub> loss from peroxy radicals formed in autoxidation is unlikely under atmospheric conditions. *The Journal of Physical Chemistry A* **2016**, *120*, 3588-3595.

The author performed all of the calculations in **Articles I, II and IV** and the majority of the calculations in **Article III**, and wrote the manuscripts.

List of other related publications:

- V Torsten Berndt, Stefanie Richters, Tuija Jokinen, **Noora Hyttinen**, Theo Kurtén, Rasmus V. Otkjær, Henrik G. Kjaergaard, Frank Stratmann, Hartmut Herrmann, Mikko Sipilä, Markku Kulmala, Mikael Ehn. Hydroxyl radical-induced formation of highly oxidized organic compounds. *Nature Communications* **2016**, 7, 13677.
- VI Siddharth Iyer, Xucheng He, **Noora Hyttinen**, Theo Kurtén, Matti P. Rissanen. Computational and experimental investigation of the detection of HO<sub>2</sub> radical and the products of its reaction with cyclohexene ozonolysis derived RO<sub>2</sub> radicals by and iodide-based chemical ionization mass spectrometer. *The Journal of Physical Chemistry A* **2017**, 121, 6778-6789.
- VII Kristian H. Møller, Rasmus V. Otkjær, **Noora Hyttinen**, Theo Kurtén, Henrik G. Kjaergaard. Cost-effective implementation of multiconformer transition state theory for peroxy radical hydrogen shift reactions. *The Journal of Physical Chemistry A* **2016**, 120, 10072-10087.

# CONTENTS

ABSTRACT

ACKNOWLEDGEMENTS

LIST OF PUBLICATIONS AND AUTHOR'S CONTRIBUTIONS

CONTENTS

LIST OF ABBREVIATION

1	INTRODUCTION.....	1
1.1	Atmospheric oxidation of VOCs .....	3
1.2	Gas-phase measurements using chemical ionization .....	7
1.3	Objectives of the thesis .....	11
2	THEORETICAL BACKGROUND .....	12
2.1	Quantum chemistry .....	12
2.1.1	Basis sets .....	13
2.1.2	Quantum chemical calculation methods.....	14
2.1.3	Thermodynamical properties .....	16
2.2	Conformer sampling .....	18
2.2.1	Hydrogen bonded complexes .....	23
2.3	Clustering simulations .....	24
2.4	Reaction rate coefficients .....	26
3	RESULTS .....	28
3.1	Lowest free energy cluster conformers .....	28
3.2	Formation free energies.....	29
3.3	Deprotonation.....	31
3.4	Fluoride transfer .....	32
3.5	Unimolecular HO <sub>2</sub> loss.....	34
4	SUMMARY AND CONCLUSIONS OF THE INDIVIDUAL RESEARCH ARTICLES .....	36

4.1	Article I: Cluster stabilities with $\text{NO}_3^-$ .....	36
4.2	Article II: Cluster stabilities with $\text{NO}_3^-$ and $\text{CH}_3\text{C}(\text{O})\text{O}^-$ .....	36
4.3	Article III: Chemical ionization with different reagent ions .....	38
4.4	Article IV: Concerted $\text{HO}_2$ loss in autoxidation reactions .....	39
	Computational tools: a review of the used software .....	40
	REFERENCES .....	41



## LIST OF ABBREVIATIONS

ACDC	Atmospheric cluster dynamics code
APi	Atmospheric pressure interface
APi-TOF	Atmospheric pressure interface time-of-flight mass spectrometer
BO	Born-Oppenheimer approximation
CI-API-TOF	Chemical ionization atmospheric pressure interface time-of-flight mass spectrometer
CIMS	Chemical ionization mass spectrometer
CCN	Cloud condensation nuclei
CDC	Collisional dissociation chamber
CI	Configuration interaction
CC	Coupled cluster
DFT	Density functional theory
GTO	Gaussian type orbital
HQTST	Harmonic quantum transition state theory
HF	Hartree-Fock
IPCC	Intergovernmental Panel on Climate Change
IMR	Ion-molecule reaction
KS-DFT	Kohn-Sham density functional theory
MBPT	Many-body perturbation theory
MESMER	Master equation solver for multi-energy well reactions
MMFF	Merck molecular force field
MP	Møller-Plesset
PNO	Pair natural orbital
PAO	Projected atomic orbital
PTR-MS	Proton transfer reaction mass spectrometer
QMS	Quadrupole mass spectrometer
RRKM	Rice-Ramsperger-Kassel-Marcus theory
RRHO	Rigid rotor harmonic oscillator approximation

SOA	Secondary organic aerosol
STO	Slater type orbital
TOF	Time-of-flight mass spectrometer
TST	Transition state theory
VOC	Volatile organic compound

# 1 INTRODUCTION

The tropospheric air consists mainly of nitrogen and oxygen. The remaining 1 % consists of various small inorganic gas compounds, such as argon gas, CO<sub>2</sub> and H<sub>2</sub>, but also of pollutants and other emissions that vary locally due to their short lifetimes in the atmosphere. These include organic and inorganic compounds emitted by both anthropogenic and biogenic sources. The inorganic compounds include small, reactive pollutants that take part in the oxidation processes in the atmosphere, such as NO<sub>x</sub>, HO<sub>x</sub> and O<sub>3</sub>.<sup>1</sup> The organic compounds are generally emitted into the atmosphere as volatile organic compounds (VOCs) by vegetation and anthropogenic sources.<sup>2,3</sup>

VOCs can be oxidized in the troposphere by several common oxidants to form less volatile, oxygenated compounds.<sup>4</sup> The three most abundant oxidants in the troposphere are O<sub>3</sub>, OH and NO<sub>3</sub>.<sup>5</sup> The dominant oxidant depends on the time of day.<sup>6</sup> For instance, the OH radical is produced by the photolysis of O<sub>3</sub> making OH present only during the daytime. After the initial oxidation by one of the oxidants, O<sub>2</sub> quickly adds to form a peroxy radical (RO<sub>2</sub>) intermediate.<sup>7</sup> The oxidation reaction chain can be terminated through bimolecular reactions of the RO<sub>2</sub> intermediate with other radical species in the atmosphere, for instance with HO<sub>2</sub> or NO, to form a hydroperoxide (ROOH) or an organic nitrate (RONO<sub>2</sub>), respectively.<sup>8-10</sup> In rare cases, some VOCs can undergo autoxidation where the number of oxygen atoms in the molecule increases by a sequence of intramolecular hydrogen shifts (H-shifts) and O<sub>2</sub> additions.<sup>11-13</sup> Autoxidation is common especially in unpolluted environments, where the bimolecular reactions that compete with the intramolecular H-shifts are less frequent due to the lack of air pollutants.<sup>12</sup> However, the reduction of anthropogenic emissions, in the effort to clean the atmosphere, has led to changes in the autoxidation reaction mechanisms of VOCs, which has resulted in the increase of highly oxygenated organic compounds in urban environments.<sup>14</sup>

Autoxidation reactions generally produce a large number of different oxygenated compounds that contain multiple functional groups.<sup>13</sup> The different chemical structures have different properties, such as saturation vapour pressure, even

if their elemental compositions are similar.<sup>15</sup> Highly oxygenated, less volatile organic compounds can take part in the formation of secondary organic aerosol (SOA) particles in the gas phase.<sup>13</sup> Based on current theoretical and experimental understanding, the formation of SOA is initiated by the clustering of acidic molecules, such as sulfuric acid<sup>16-20</sup> ( $\text{H}_2\text{SO}_4$ ) or iodic acid<sup>21</sup> ( $\text{HIO}_3$ ), and basic molecules, such as ammonia<sup>22-25</sup> ( $\text{NH}_3$ ) or dimethylamine<sup>26,27</sup> ( $(\text{CH}_3)_2\text{NH}$ ). Once a cluster is large enough, oxygenated organic compounds with low volatilities are able to condense onto the particle growing it more rapidly.<sup>13</sup>

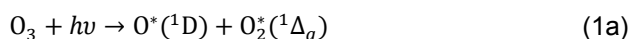
Aerosol particles have both cooling and warming effects on the climate but according to the most recent Intergovernmental Panel on Climate Change (IPCC) assessment report,<sup>28</sup> the effect of aerosol on the earth's radiative forcing is still uncertain. Depending on the properties of the aerosol and the environmental conditions, aerosol can scatter or absorb sunlight. Scattering aerosol has a cooling effect, as it increases the reflectivity of the Earth, and absorbing aerosol (mainly black carbon) has a warming effect. An additional, indirect cooling effect of aerosol is caused by cloud droplet formation that originates from aerosol particles. If aerosol particles are able to grow to larger sizes faster than they evaporate, they can become cloud condensation nuclei (CCN). This is more likely to happen in cases where the addition of molecules to the cluster is faster than the evaporation from the cluster. A larger number concentration of CCN leads to clouds with smaller water droplets that reflect more sun light back to space.<sup>28</sup> However, the total effect of clouds with smaller droplets is uncertain, as the smaller droplets are more likely to evaporate, but at the same time, higher aerosol concentration supposedly suppresses rainfall.<sup>28</sup>

Current models on cluster formation and growth are unable to reproduce cluster concentrations measured in chamber studies.<sup>29,30</sup> One reason for the difference between theory and experiments is that the models are unable to simulate the behaviour of the clusters inside the instruments. In addition, most neutral molecules with very low, atmospherically relevant concentrations, cannot be directly measured from the gas-phase and the indirect measurement techniques have uncertainties. Many gas-phase measurements have been done using mass spectrometers, which are able to determine only the elemental composition of molecules, not the different structural isomers. Theoretically, reaction rates of gas-

phase reactions can be calculated using quantum chemistry to help with the identification of possible chemical structures of measured molecular masses. The work in this thesis focuses on using quantum chemistry to calculate the rate of a reaction that has been used to explain a certain molecular mass in gas phase measurements (**Article IV**) and to model the differences in measurements of neutral molecules in the gas-phase (**Articles I-III**).

## 1.1 Atmospheric oxidation of VOCs

The dominating oxidant in the troposphere varies depending on the time of day. The OH radical is formed by the photolysis (wavelengths < 310 nm) of O<sub>3</sub>:



and is only formed in sunlight. In addition, the NO<sub>3</sub> radical is photo dissociated by sunlight which means that it is generally present only during night time. However, NO<sub>3</sub> has been measured during the daytime in polluted environments, where the formation rate of NO<sub>3</sub> is higher than the dissociation rate.<sup>31-33</sup> Ozone is produced by anthropogenic sources, and by the photolysis (wavelengths < 400 nm) of NO<sub>2</sub>:



where M is a molecule (usually N<sub>2</sub>) that takes away the excess energy of the association reaction. Ozone can also be transported to the troposphere from the stratosphere, where O is formed by the photolysis (wavelengths < 242 nm) of oxygen molecules:



and in combination with Reaction (2b), forms O<sub>3</sub>.<sup>5</sup> Due to its anthropogenic sources and longer lifetime, compared to OH and NO<sub>3</sub>, O<sub>3</sub> is present in the troposphere during day- and nighttime with varying concentrations. Oxidation initiated by the different oxidants leads to products with different functional groups. Most commonly, O<sub>3</sub> initiated oxidation leads to product compounds that contain acid

groups,<sup>34</sup> OH initiated oxidation produces hydroxides<sup>35</sup> and the addition of NO<sub>3</sub> leads to nitrooxy group (-ONO<sub>2</sub>) containing products.<sup>36,37</sup>

The first steps of alkene ozonolysis are fairly well known.<sup>38</sup> The ozone molecule attacks a double bond in the VOC forming a primary ozonide. The ozonide then decomposes into a Criegee intermediate which can, among other reactions, isomerize to a vinyl hydroperoxide that can dissociate into a carbon-centred radical by losing an OH radical. In endocyclic compounds, the breaking double bond leads to the breaking of the ring, but in non-endocyclic alkenes, the decomposition of the ozonide will break the carbon chain leading to a closed-shell carbonyl product and (after Criegee intermediate isomerization and OH loss) a carbon-centred radical intermediate. At atmospheric oxygen concentrations, oxygen quickly adds to the carbon-centred radical creating an RO<sub>2</sub> radical.<sup>39</sup> In polluted conditions, several different bimolecular reactions with, for instance, NO or HO<sub>2</sub> can terminate the radical reaction chain of the organic molecule to form a closed-shell product.

In unpolluted conditions the reaction chain can continue as autoxidation, an example of an autoxidation reaction mechanism of cyclohexene is shown in Figure 1. In autoxidation, a new carbon-centred radical is formed when the RO<sub>2</sub> radical (formed from the O<sub>2</sub> addition) abstracts a hydrogen from one of the carbon atoms. If the molecule has aldehydic carbons, the hydrogen is generally most easily abstracted from those,<sup>11,39</sup> and the next O<sub>2</sub> addition and the following intramolecular H-shift will form a carbon-centred radical intermediate that contains a peroxy acid group (-C(O)OOH). The O<sub>2</sub> additions to carbon radical centres and intramolecular H-shifts can rapidly increase the number of oxygen atoms in the molecule if the intramolecular H-shift reactions are fast enough to compete with bimolecular reactions. In addition, rapid intramolecular H-shifts<sup>40,41</sup> between the peroxy radical and a hydroperoxy group (-OOH) can affect which hydrogen is most likely to be abstracted and consequently where the next O<sub>2</sub> is added. The effect of additional complexity of the VOC on the autoxidation mechanism has also been studied computationally using methylcyclohexene and  $\alpha$ -pinene.<sup>42,43</sup>

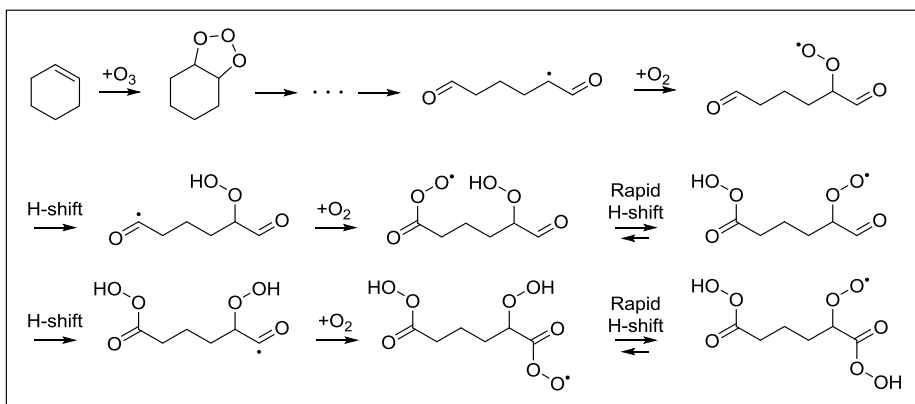


Figure 1 - Ozone initiated autoxidation of cyclohexene<sup>39</sup> with additional rapid H-shifts.<sup>41</sup>

In the OH radical initiated oxidation, OH commonly adds to a C-C double bond of an unsaturated VOC, adding a hydroxy group (-OH) to the molecule, instead of the carbonyl groups (=O) formed in ozonolysis. Generally, the addition of  $O_2$  molecules leads to the formation of hydroperoxy groups rather than peroxy acid groups (see Figure 2), unless the initial reactant contains an aldehyde group (-CHO). The oxidation of isoprene has been widely studied,<sup>35,44-47</sup> as isoprene is abundant in the troposphere. Figure 2 shows various oxidation and autoxidation mechanisms of isoprene starting from the initial oxidation step and the addition of oxygen. After the OH addition, the radical centre is delocalised due to the second double bond and the oxygen can add to two different positions leading to different structural isomers.

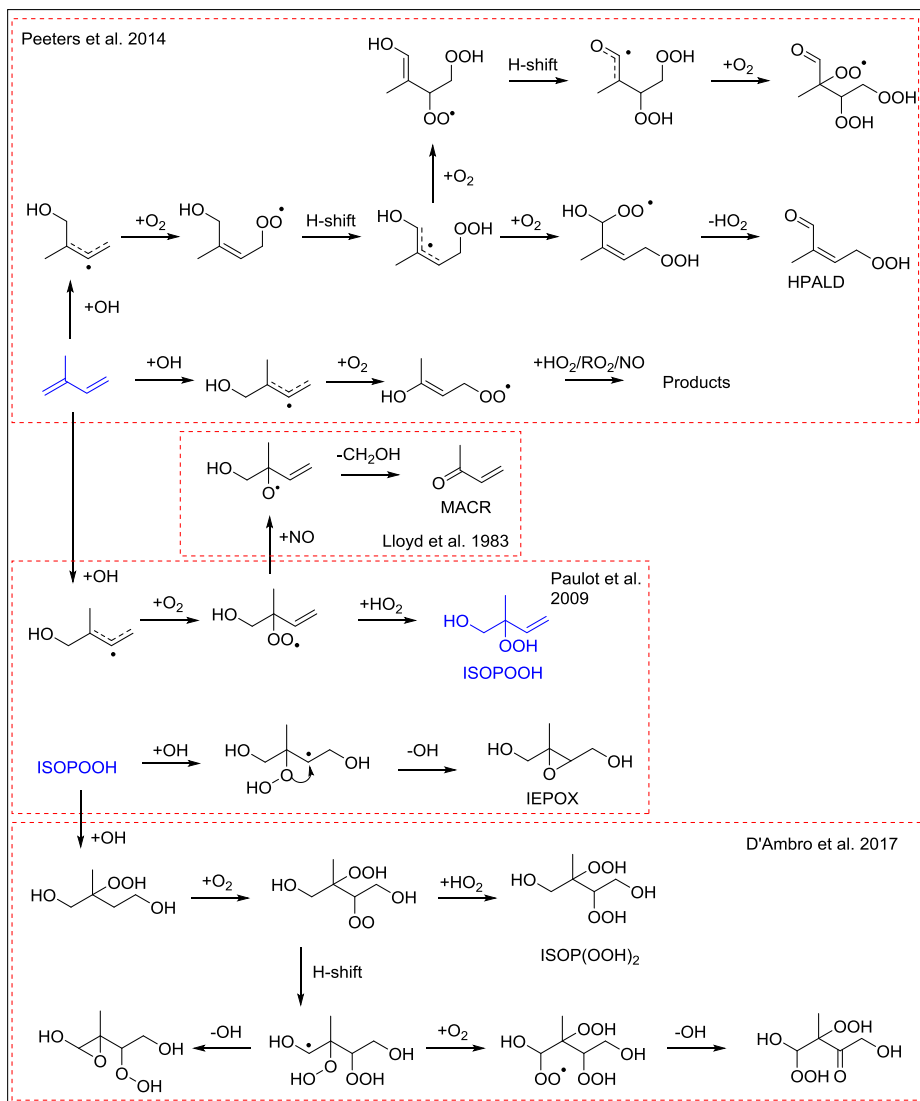


Figure 2 – Some of the major mechanisms in OH-initiated oxidation of isoprene.<sup>44-47</sup> More oxidation mechanisms can be found in Wennberg et al.<sup>35</sup>



## 1.2 Gas-phase measurements using chemical ionization

Oxidized organic molecules in the ambient air are often detected using mass spectrometers. The advantages of mass spectrometry include high-resolution and the ability to measure small concentrations of trace gases. The detection occurs at low pressure (around  $10^{-6}$  mbar) but using Atmospheric Pressure Interface Time-of-Flight (APi-TOF<sup>48</sup>) mass spectrometers, the molecules can be sampled directly from the ambient air under atmospheric pressures without sample preparation. The APi then lowers the pressure inside the instrument down to near vacuum pressures of the TOF. Unlike quadrupole mass spectrometers (QMS), TOF mass spectrometers are able to separate isobaric molecules with the same unit mass.

There is a disadvantage in mass spectrometers because only charged species can be detected since in the instrument, the gas phase ions and charged clusters are guided to a detector using an electric field. For this reason, neutral molecules need to be charged before they can be detected. Neutral molecules can be charged using chemical ionization, where the sample molecule is ionized by clustering, charge transfer or other chemical reactions with reagent ions. Other ionization methods include, for instance, photoionization, electrospray ionization, electron impact ionization, fast atom bombardment, matrix assisted laser desorption ionization, and sonic spray ionization. Figure 3 shows the most common chemical ionization processes with acetate ( $\text{CH}_3\text{C}(\text{O})\text{O}^-$ ) as the reagent ion and a highly oxidized product of cyclohexene ozonolysis as the sample molecule.

Anion chemical ionization is often used for the detection of neutral oxidized organic compounds. When clustering with sample molecules, the negative reagent ions act as hydrogen bond acceptors (e.g. the oxygen atoms of  $\text{CH}_3\text{C}(\text{O})\text{O}^-$  in Figure 3) forming hydrogen bonds to the hydrogen bond donating functional groups of the sample molecule (e.g. the peroxy acid groups in Figure 3). Generally the formed ion-molecule cluster is lower in energy than the separate reagent ion and sample molecule. The ion-molecule cluster can then be detected using a mass spectrometer.

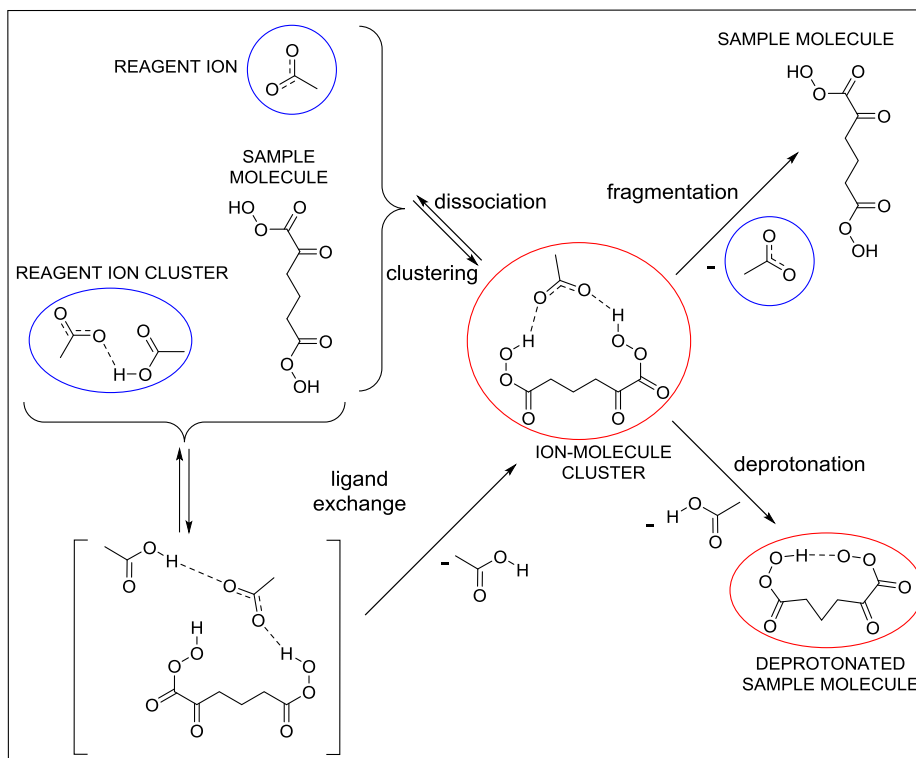


Figure 3 - Anion chemical ionization processes. The circled species are negatively charged and can thus be detected by the mass spectrometer.

If the reagent ion is already clustered with another neutral molecule, the sample molecule can be charged via a ligand exchange reaction, shown in Figure 3. This is common, for instance, when the nitrate ion ( $\text{NO}_3^-$ ) is used as the reagent ion. In the instrument,  $\text{NO}_3^-$  ions are produced by ionizing nitric acid ( $\text{HNO}_3$ ). As only a fraction of  $\text{HNO}_3$  is ionized, the remaining acid is able to cluster with the  $\text{NO}_3^-$  ions. The binding of the sample molecule to this reagent ion cluster is generally not strong enough for the  $\text{HNO}_3 - \text{NO}_3^- - \text{sample molecule}$  cluster to be detected by the mass spectrometers.<sup>49</sup> Assuming that the cluster fragments in the instrument, the most probable fragmentation path way is the one where the ion-molecule cluster is more strongly bound. The probability of the ligand exchange reaction depends on the binding strengths of the reagent ion cluster (e.g.,  $\text{HNO}_3(\text{NO}_3^-)$ ) and the forming ion-molecule cluster. If the reagent ion cluster is energetically very stable, as the  $\text{HNO}_3(\text{NO}_3^-)$  cluster is, the sample molecule is likely not ionized.

Anion chemical ionization is a relatively soft ionization method, meaning that the reagent ion generally does not break up the sample molecules. Some reagent ions, however, can charge the sample molecules through various chemical reactions. For instance reagent ions, such as  $\text{CH}_3\text{C}(\text{O})\text{O}^-$ ,  $\text{NO}_3^-$  and  $\text{I}^-$ , are able to abstract a positively charged fragment from the sample molecule leaving a negatively charged product. These reactions include H, OH and O abstraction from an acid group of the sample molecule. An example of a proton transfer (deprotonation) by  $\text{CH}_3\text{C}(\text{O})\text{O}^-$  is shown in Figure 3.

Anion chemical ionization has been used in several atmospheric measurements using, for instance,  $\text{NO}_3^-$ ,<sup>13,30,50-52</sup>  $\text{CF}_3\text{O}^-$ ,<sup>53-56</sup> and  $\text{I}^-$ <sup>57-59</sup> as reagent ions. The  $\text{NO}_3^-$  anion is selective toward molecules with high oxygen content, due to its strong binding with  $\text{HNO}_3$ . The  $\text{CF}_3\text{O}^-$  anion was originally used to detect small inorganic compounds in the atmosphere due to its ability to react with molecules to form negatively charged product molecules (through fluoride transfer or other reactions).<sup>60</sup> The  $\text{I}^-$  anion is able to charge a variety of atmospherically relevant molecules<sup>59</sup> but  $\text{I}^-$  measurements have high humidity dependence<sup>61</sup> (presumably caused by the formation of  $(\text{H}_2\text{O})_n\text{I}^-$  clusters) which causes problems in the varying relative humidity of the atmosphere.

Cation chemical ionization is often used in proton transfer reaction mass spectrometers (PTR-MS), which commonly use  $\text{H}_3\text{O}^+$  as the reagent ion. Other possible reagent cations include  $\text{NH}_4^+$ ,  $\text{NO}^+$ ,  $\text{O}_2^+$ ,  $\text{Xe}^+$  and  $\text{Kr}^+$ . The sample molecules are charged through proton or charge transfer reactions. For the proton transfer to work, the proton affinity of the sample molecule needs to be higher than that of, for instance water, when  $\text{H}_3\text{O}^+$  is the reagent ion. PTR-MS methods are most commonly used to measure less oxygenated molecules that cannot be detected using anion chemical ionization. In atmospheric measurements, PTR-MS has been used to measure VOCs<sup>62-65</sup> and amines<sup>66</sup> using  $\text{H}_3\text{O}^+$ . In addition,  $\text{NH}_4^+$  has recently been used to detect oxidized molecules as  $\text{NH}_4^+$  clusters.<sup>67</sup>

There are many factors that affect how well the molecules can be detected by a chemical ionization mass spectrometer (CIMS). The collision rates and ligand exchange rates affect how efficiently the sample molecules are charged in the ion-molecule reaction (IMR) region of the instrument where the reagent ions and the

sample molecules are mixed together. The chemical reactions, such as deprotonation, occurring in the IMR region do not affect the overall chemical ionization efficiency, as both the clusters and the products of the reactions can be detected by the instrument. However, analysing a spectrum with both clusters and deprotonated sample molecules is more complicated than analysing a spectrum of only clusters, which may lead to errors in the analysis.

In the ion optics of the instrument, the pressure decreases and the speed of the ions and clusters increases. In this region, some of the ion-molecule clusters can be fragmented due to high velocity collisions. The clusters can also dissociate in the IMR region if the cluster formation is very exothermic and the collisional stabilization of the cluster is not efficient enough. The cluster can fragment back to the original sample molecule and reagent ion, or other products depending on the how energetic the collisions are. If the cluster fragments back into the neutral sample molecule and the reagent ion, the information of the sample molecule is lost, as only the reagent ion is detected by the instrument. Other fragmentation products can still be detected by the instrument, as long as the charge remains with the sample molecule. The most probable fragmentation pathway is the one with the most stable (energetically favourable) products.

The reagent ion for measurements is selected based on the target molecules that the user wants to detect. The  $\text{NO}_3^-$  anion is highly selective toward highly oxidized molecules as  $\text{HNO}_3(\text{NO}_3^-)$  clusters are more stable than the ion-molecule clusters of less oxidized sample molecules. For measuring only acidic compounds,  $\text{CH}_3\text{C}(\text{O})\text{O}^-$  is a good option, as it is able to deprotonate molecules that have higher gas-phase acidities than acetic acid ( $\text{CH}_3\text{C}(\text{O})\text{OH}$ ). For measuring only deprotonation products, the ion-molecule clusters can be dissociated using a collisional dissociation chamber (CDC) after the IMR region,<sup>68</sup> which leads to deprotonation of acids, and fragmentation into reactants for any other clusters.

If the sensitivity of the CIMS instrument toward a specific molecule is known, the instrument can be used to measure concentrations of the compound accurately. The sensitivity of a compound can be measured for different reagent ions if the pure compound is available. The calibration of the instrument in measurements of sample molecules that cannot be synthesized (like most autoxidation products) has challenges, since the sensitivities of the molecules are unknown. In these

cases, the sensitivities need to be estimated and, therefore, the analysis of the measurements is less reliable. In  $\text{NO}_3^-$  measurements, for instance, the instrument is often calibrated using  $\text{H}_2\text{SO}_4$ , with the assumption that  $\text{H}_2\text{SO}_4$  can be detected at the maximum sensitivity. A calibration factor is then calculated for  $\text{H}_2\text{SO}_4$ , and the same factor is used to calculate an upper limit estimate for the concentrations of other sample molecules.

The detection efficiencies of different reagent ions have been studied mainly in laboratory experiments in order to find a reagent ion or measurement technique that is able to measure accurate concentrations of trace gases from the ambient air. Currently, experiments on highly oxidized closed-shell products and  $\text{RO}_2$  intermediates of atmospherically relevant alkenes have shown that  $\text{CH}_3\text{C}(\text{O})\text{O}^-$  has higher detection efficiency than  $\text{NO}_3^-$ , and that lactate ( $\text{CH}_3\text{CH}(\text{OH})\text{C}(\text{O})\text{O}^-$ ) and pyruvate ( $\text{CH}_3\text{C}(\text{O})\text{C}(\text{O})\text{O}^-$ ) have detection efficiencies close to, or lower than,  $\text{CH}_3\text{C}(\text{O})\text{O}^-$ .<sup>69-71</sup>

### 1.3 Objectives of the thesis

The main objectives of this thesis are to:

- Use computational chemistry to explain the differences in detection efficiencies of  $\text{NO}_3^-$  and  $\text{CH}_3\text{C}(\text{O})\text{O}^-$  in the chemical ionization measurements of highly oxygenated  $\text{RO}_2$  intermediates and closed-shell products of cyclohexene ozonolysis.
- Computationally compare different reagent ions that have not been compared experimentally. This can help in analysing experimental results and selecting reagent ions for detecting oxidized organic molecules.
- Investigate a unimolecular  $\text{HO}_2$  loss reaction that has been proposed for autoxidation reactions based on observed elemental compositions. A concerted  $\text{HO}_2$  loss reaction is known to occur in smaller molecules under atmospheric conditions but has not been reported for larger, atmospherically relevant molecules.

## 2 THEORETICAL BACKGROUND

### 2.1 Quantum chemistry

In quantum chemistry, the properties of molecules can be calculated from the wave function ( $\psi$ ) of the system (atom/molecule/group of molecules) by solving the time-dependent Schrödinger equation:

$$\hat{H}\psi = i \frac{\partial\psi}{\partial t}, \quad (3)$$

where  $\hat{H}$  is the Hamiltonian operator of the system and  $t$  is time. The Hamiltonian operator includes terms for both the kinetic energy ( $\hat{T}$ ) and the potential energy ( $\hat{V}$ ):

$$\hat{H} = \hat{T} + \hat{V} \quad (4)$$

The kinetic energy operator is a sum of the kinetic operators of all particles, i.e.,  $\hat{T}_n$  and  $\hat{T}_e$  for nuclei and electrons, respectively. The potential energy operator includes all interactions between all particles ( $\hat{V}_{nn}$ ,  $\hat{V}_{ne}$  and  $\hat{V}_{ee}$ ). Assuming that the potential energy operator is time-independent, the whole Hamiltonian becomes time-independent. This way the time and space variables of the wave function can be separated. The time dependence can be written as a phase factor that is multiplying the spatial wave function. The phase factor is neglected to obtain the time-independent Schrödinger equation:

$$\hat{H}\psi = E\psi, \quad (5)$$

where  $E$  is the energy of the system in the ground state.

To solve the Schrödinger equation, some approximations are needed. These approximations lead to inaccuracies in the results, but solving the Schrödinger equation without any approximations is impossible for a system containing multiple nuclei and electrons. The motion of the nuclei and electrons can be separated using the Born-Oppenheimer approximation. From the point of view of the electrons, the nuclei are stationary, since the electrons are much lighter and faster than the nuclei. This enables solving the electronic and the nuclear wave function of the system separately:

$$\hat{H} = \hat{H}_{nuc} + \hat{H}_{el} \quad (6)$$

### 2.1.1 Basis sets

In quantum chemical methods, the wave function of the system is formed from non-interacting one-electron wave functions. Each one-electron wave function (i.e., molecular orbital,  $\phi$ ) can be written as a linear combination of basis functions ( $\chi$ ):

$$\phi = \sum_i a_i \chi_i, \quad (7)$$

where the coefficients  $a$  are solved in the calculation. There are two different types of basis functions: Slater type orbitals (STOs) and Gaussian type orbitals (GTOs). The STOs are of the same mathematical form as the orbitals of the hydrogen atom:

$$\chi_{\zeta,n,l,m}(r, \theta, \varphi) = N Y_{l,m}(\theta, \varphi) r^{n-1} e^{-\zeta r}, \quad (8)$$

where  $N$  is a normalization constant,  $Y_{l,m}$  are spherical harmonic functions depending on the angular momentum quantum numbers  $l$  and  $m$ ,  $n$  is the principle quantum number,  $\zeta$  is an exponent controlling the width of the orbital and  $r$ ,  $\theta$  and  $\varphi$  are the polar coordinates. The GTOs are approximations of the orbitals of the hydrogen atom:

$$\chi_{\zeta,n,l,m}(r, \theta, \varphi) = N Y_{l,m}(\theta, \varphi) r^{2n-2-l} e^{-\zeta r^2} \quad (9)$$

The most commonly used basis functions of the two are GTOs, due to the difficulties in the STO calculations when the number of basis functions increases. In addition, GTOs can be used to approximate STOs by creating contracted basis functions, which are linear combinations of GTOs.

A basis set defines how many basis functions are used to describe each atomic or molecular orbital in the wave function of the system. The minimum basis set includes the smallest number of basis functions needed to describe the system, and more basis functions can be added to increase the accuracy of the computations. The minimum basis set for the hydrogen atom includes only one basis function for the s-orbital. In addition to the s-functions, the minimum basis set of the first row elements includes a set of functions for the p-orbitals. The first improvement to the minimum basis set is to multiply the number of basis functions. For instance, in a Double Zeta (DZ) basis set the number of basis functions has been doubled from the minimum basis set. However, it is generally useful to multiply

only the basis functions describing the valence orbitals, and not the core orbitals. This leads to the use of split valence basis sets, e.g. VDZ.

Additional basis functions are needed to describe the bonding in molecules. To describe covalent bonds, basis functions corresponding to one quantum number higher angular momentum than the valence orbitals of all atoms are added to the basis set. These polarization functions are denoted with p or P in the basis set name. In addition, diffuse functions are needed to describe hydrogen bonds and anions. Using diffuse functions, the part of the atomic orbital that is farther from the nucleus is described by using small exponents ( $\zeta$ ) in the basis function. In the basis set names, diffuse functions are denoted with + or aug. In theory, the increase in the basis set size (i.e., going from DZ to Triple Zeta (TZ) or higher (QZ, 5Z, 6Z...), or the addition of polarization and diffuse functions) should lead to more accurate calculations.

### 2.1.2 Quantum chemical calculation methods

There are two main groups of quantum chemical calculation methods that can be used for solving the Schrödinger equation: wave function -based methods and density functional theory (DFT) methods. In DFT methods, the non-interacting one-electron wave functions are used to form the electron density of the system, which in turn determines the energy of the system in the ground electronic state. The Schrödinger equation is then solved using the Kohn-Sham (KS-DFT) equations:

$$E_{DFT} = T_s + V_{ne} + V_{ee} + E_{xc}, \quad (10)$$

where the kinetic energy functional ( $T_s$ ), the classical coulombic attraction between the nuclei and electrons ( $V_{ne}$ ) and repulsion between electrons ( $V_{ee}$ ), and the exchange-correlation functional ( $E_{xc}$ ) are all functionals of the electron density. The exchange-correlation functional yields the exchange and correlation energies. To fulfil the Pauli Exclusion Principle, the total wave function of the system has to be antisymmetric. In DFT methods, the exchange energy is a correction to the classical Coulomb interaction between the electrons ( $V_{ee}$ ) to account for the antisymmetry. The correlation energy is needed to account for the fact that the motion of the electrons is correlated. The exchange-correlation term is thus a correction to



approximations made in the kinetic and potential energies. With the true exchange-correlation functional the total electronic energy would be exact. Unfortunately,  $E_{xc}$  is unknown, which means that the correlated and non-correlated energies cannot be calculated separately.

In wave function methods, the one-electron wave functions are combined to form a Slater determinant. The Schrödinger equation is then solved using the Hartree-Fock (HF) method. Since a Slater determinant is always antisymmetric, the HF method includes the exact exchange energy and it does not need to be included separately. In the HF method, the electron-electron repulsion is included as a mean field, which is the average effect of all other electrons on the electron. The equations are solved iteratively by minimizing the energy of the system since, according to the variational principle, the energy calculated using the HF method is always higher than the actual energy of the system.

The HF method excludes electron correlation, which means that it is unable to find the exact energy of the system. In post-HF methods, the electron correlation is calculated separately as a correction to the HF electronic energy. Post-HF methods include Configuration Interaction (CI), Coupled Cluster (CC) and Many-Body Perturbation Theory (MBPT) methods. In the CI methods, the wave function is constructed as a sum of the HF Slater determinant and determinants that describe excited states relative to the HF Slater determinant. Like the HF method, the CI methods can be solved variationally. In the CC methods, the HF wave function is multiplied with the exponential cluster excitation operator. The CC wave function can also be solved variationally but the calculation is possible only for small systems.<sup>72</sup> That is why the CC methods are generally not variational. In the MBPT methods, the electron correlation is calculated using an additional perturbation part in the Hamiltonian operator. The most commonly used perturbation theory method is the Møller-Plesset (MP) perturbation theory. Instead of excitations, MBPT methods use different orders of perturbation to correct the uncorrelated energy. The zeroth order solution is equal to the unperturbed solution. Since the MBPT methods are not variational, the increase in the order of the theory does not necessarily lead to more accurate results.

The commonly used highly accurate post-HF method is the canonical coupled cluster method, CCSD(T), where the electron correlation is calculated using

single and double excitations and perturbative treatment of triple excitations. This method is feasible only for small systems (<400 basis functions<sup>73</sup> when the system has no symmetry) due to the  $N^7$  (where  $N$  is the size of the system defined by the number of basis functions) scaling of the calculation time. Compared to standard canonical coupled cluster methods, the F12 coupled cluster methods have an improved basis set convergence<sup>74</sup> due to additional inter-electronic distances included in the methods. Therefore, smaller basis sets are needed to achieve the same accuracies as in the standard CC methods. In addition, a recent development in local correlation methods, a domain-based local pair natural orbital approximation (DLPNO<sup>75</sup>), has a near-linear scaling making it suitable for even large systems. The DLPNO method is a combination of pair natural orbitals (PNOs) and projected atomic orbitals (PAOs) to create a more accurate and faster computational method.<sup>76</sup> Unlike in the canonical coupled cluster methods, the DLPNO coupled cluster methods calculate the excitations locally. The DLPNO-CCSD(T) method is able to recover more than 99.6 % of the correlation energy of the canonical CCSD(T).<sup>75</sup>

### 2.1.3 Thermodynamical properties

In a simple model, thermodynamic properties of a system can be calculated using the partition functions ( $q$ ) of the electronic, translational, vibrational and rotational degrees of freedom. The total partition function ( $Q$ ) is the product of these four factors. The enthalpy ( $H_X$ ) and entropy ( $S_X$ ) of each factor can be calculated using the partition function of the factor using Equations (11) and (12), respectively.

$$H_X = k_B T^2 \left( \frac{\partial \ln q_X}{\partial T} \right)_V + k_B T V \left( \frac{\partial \ln q_X}{\partial V} \right)_T \quad (11)$$

$$S_X = k_B T \left( \frac{\partial \ln q_X}{\partial T} \right)_V + k_B \ln q_X \quad (12)$$

Here  $q_X$  is the partition function of either translational, vibrational, electronic or rotational degree of freedom,  $k_B$  is the Boltzmann constant,  $T$  is the temperature and  $V$  is the volume. The total enthalpy ( $H$ ) and entropy ( $S$ ) of the system are the sums of the contributions of each four factors. Gibbs free energies ( $G$ ) can be calculated approximately from the entropy and enthalpy of the system:

$$G = H - TS \quad (13)$$

The zero-point corrected energy (potential energy) can be calculated as a sum of the electronic energy and the zero-point energy correction ( $E_{z-p}$ ), which is calculated from the sum of all vibrational frequencies  $\nu_i$  of the system:

$$E_{z-p} = \frac{1}{2} h \sum_i \nu_i, \quad (14)$$

where  $h$  is the Planck constant.

Vibrational frequencies are generally calculated using the rigid rotor harmonic oscillator (RRHO) approximation, which assumes that all rotational modes are rigid and all vibrational modes of the system are harmonic. In addition, ideal gas is assumed when computing the translational partition function. However, the RRHO approximation is not always appropriate for all vibrational degrees of freedom of larger molecules and especially for hydrogen bonded clusters. Since the formation energies are calculated as the difference between the cluster and the free molecule, the error from the anharmonic vibrations of the separate molecules is cancelled out. However, the error from the anharmonic vibrations of the cluster remains.

In this thesis, the Gibbs free energies and zero-point corrected energies were calculated using a DFT functional,  $\omega$ B97xD,<sup>77</sup> and the aug-cc-pVTZ<sup>78</sup> basis set for the geometry optimization and harmonic frequency calculations. The  $\omega$ B97xD functional is a long-range corrected hybrid density functional that includes empirical atom-atom dispersion corrections. The basis set is a correlation-consistent (cc), Valence Triple Zeta basis set with diffuse functions (aug) on heavy atoms (non-hydrogen atoms) and a set of polarization functions (p). The cc basis sets are especially designed to recover the correlation energy of the valence electrons in post-HF methods. In addition, a lower level method, B3LYP/6-31+G\*, was used for single-point energy calculations and geometry optimizations in the conformer sampling. The B3LYP (Becke, three-parameter, Lee-Yang-Parr) functional is commonly used. It includes the Becke-3-parameter exchange functional and Lee-Yang-Parr correlation functional.<sup>79-81</sup> The symbol 6-31+G\* denotes for a split valence basis set, which includes one contracted basis function (with six GTOs) for the core orbitals, and two contracted basis functions (with three and one GTOs)

for the valence orbitals. The basis set also has one set of diffuse functions (+) and a set of polarization functions for all non-hydrogen atoms (\*).

Two different post-HF wave function-based methods were used to calculate the electronic energies. The DLPNO-CCSD(T)<sup>75,76</sup> method with def2-QZVPP<sup>82,83</sup> basis set (which is an Ahlrichs type basis set) was used to calculate the single-point energies of closed-shell molecules and clusters, and as the DLPNO method was at the time not available for open-shell molecules, the electronic energies of radicals were calculated with the CCSD(T)-F12<sup>84</sup> method using the VDZ-F12<sup>85-87</sup> basis set. The difference between the VDZ-F12 basis set and the complete basis set limit has been found to be on average 0.42 kJ/mol when calculating the electronic formation energies of hydrogen bonding complexes.<sup>88</sup> Comparing the chemical ionization reaction energies in **Article III**, we found on average 0.55 kJ/mol difference between the CCSD(T)-F12/VDZ-F12 and the DLPNO-CCSD(T)/def2-QZVPP levels of theory.

## 2.2 Conformer sampling

Large and flexible molecules have multiple conformers (local minima on the potential energy surface). Figure 4 shows, as an example, six different conformers of lactic acid ( $\text{CH}_3\text{CH}(\text{OH})\text{C}(\text{O})\text{OH}$ ). These conformers have the same chemical structure but different 3-D structures (i.e., the combination of the dihedral angles in each conformer is different). This means that the molecule is able to convert to different conformers without breaking or forming covalent bonds. However, the intramolecular interactions, including hydrogen bonding, in the conformers may be different, which can lead to large energy differences between the conformers.

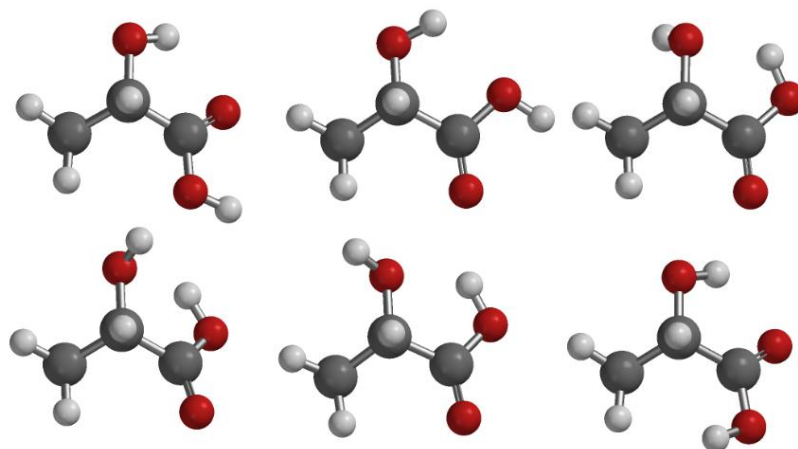


Figure 4 – Six different conformers of lactic acid. Color coding: grey = C, red = O, white = H.

Selecting an arbitrary conformer can lead to significant errors as the energy differences between different conformers can vary by several kJ/mol. In calculations, it is possible to use either only the lowest energy conformer, or a set of low energy conformers. For both of these options, all possible conformers need to be investigated to obtain the conformers with the lowest energies. Finding the lowest energy conformer of the molecule is important especially in reaction rate calculations, where even small errors in the energy barriers may lead to large errors in the reaction rate coefficients. The most accurate result can be achieved by using all possible conformers in the calculations. However, based on the Boltzmann distribution, in equilibrium conditions the majority of the individual molecules are in the low-lying energy conformations. In **Article VII** we found that it is possible to obtain accurate results using a limited number of low-energy conformers.

Lactic acid has four non-terminal bonds, i.e., four torsional angles. Rotating around the bonds changes the energy of the molecule. Generally the one-dimensional energy surfaces of organic molecules, along one dihedral angle, have 1-3 local minima. For example, rotating the hydroxy group of lactic acid has a different number of local minima depending on whether the hydroxy group is able to form an intramolecular hydrogen bond to an oxygen atom of the carboxylic acid group (-C(O)OH) or not. Figure 5 shows two different one-dimensional energy surfaces

of the rotation of the same hydroxy group in lactic acid. In the top panel, the hydrogen of the carboxylic acid group is pointing toward the rotating hydroxy group, and in the bottom panel the hydroxy group is able to form a hydrogen bond with the acid group.

All conformers (local minima on the energy surface) can be found by scanning the  $n$ -dimensional energy surface where  $n$  is the number of torsional angles. Depending on the grid size of the scan and the calculation method, these types of calculations are generally computationally too demanding for larger molecules with multiple torsional angles. In the conformer search algorithm of the Spartan '14 program,<sup>89</sup> the torsional angles are changed in steps so that all combination of the different torsional angles are checked systematically. The default step size in Spartan '14 is 120 degrees, making the energy surface sparse. However, unconstrained optimization of all the points on this energy surface gives an extensive set of conformers.

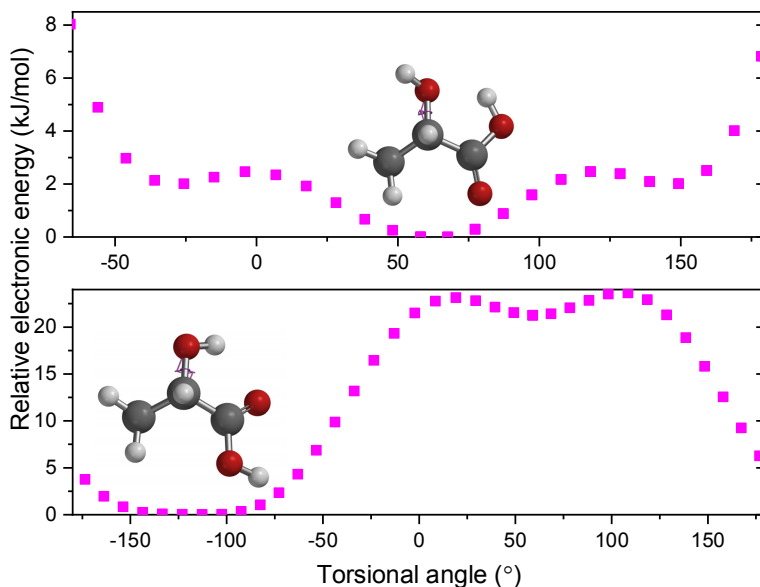


Figure 5 - One-dimensional potential energy surfaces of the hydroxy group torsion in lactic acid with two different orientations of the carboxylic acid group. The molecular structures shown represent the global minima along the 1-D energy surfaces. Color coding: grey = C, red = O, white = H.

High-level optimizations of all unique local minimum conformers would use a lot of computational time, which has led to the development and use of different computational methods aimed at reliably finding the lowest energy conformer with the least amount of used computer time. In many studies,<sup>39,41,90</sup> the initial conformers are generated using a cheap and less accurate computational method, which is able to produce geometries that are reasonably close to the actual minima. The obtained conformers can then be optimized using a DFT method, which are often reliable for calculating relative energies between different conformers of the same molecule.

The conformer sampling method that was used in **Articles I-IV** was developed for finding the lowest-energy conformers for reaction rate calculations in the autoxidation of cyclohexene.<sup>39</sup> All conformers were generated using the systematic conformer search and MMFF force fields<sup>91-95</sup> in the Spartan '14 program. In force field methods, the electronic energy of the system is solved using a parametric function of the atom coordinates. The electrons are not considered in the calculation. Instead, the interaction between the atoms of the system are described through bonded and non-bonded interactions, and the parameters in the electronic energy calculation are fit to experimental or higher level computational reference data. Unfortunately, the MMFF force field is not parametrized for radicals. In cases where the molecule is a radical, the charge of the radical centre needs to be changed to neutral to prevent artificially strong hydrogen bonding between the radical centre and hydrogen bond donating groups of the molecule. Different conformer sampling methods for RO<sub>2</sub> radicals were tested in **Article VII**, and we found that the conformer sampling of RO<sub>2</sub> radicals finds most of the low-energy conformers if the type of the radical centre oxygen is set as a C-O-C type oxygen.

The single-point electronic energies of all conformers were calculated at the B3LYP/6-31+G\* level of theory and all conformers within 20.9 kJ/mol (5 kcal/mol) of the lowest-energy conformer were optimized at the same level. Conformers within 8.4 kJ/mol (2 kcal/mol) were then optimized at a higher level of theory using the  $\omega$ B97xD functional and aug-cc-pVTZ basis set. The final electronic energy was calculated only for the lowest energy conformer either at the DLPNO-CCSD(T)/def2-QZVPP (closed-shell) or CCSD(T)-F12/VDZ-F12 (radicals) level of theory.

Figure 6 shows an example of how the number of conformers was reduced before every step of the increasingly more expensive calculations. The calculations started with finding all conformers by using a systematic search algorithm implemented in Spartan '14. The red squares in Figure 6 show the electronic energy of each conformer after a single-point energy calculation at the B3LYP/6-31+G\* level of theory. The conformers are ordered based on their original MMFF energies from the conformer search. The blue circles and black triangles are the electronic energies after a B3LYP/6-31+G\* and  $\omega$ B97xD/aug-cc-pVTZ geometry optimization, respectively. In this example, the number of conformers is only 26, so the high-level calculations could have been done to all conformers. With larger molecules and clusters, the number of conformers is larger, and the cut-offs are more important to conserve computer time.

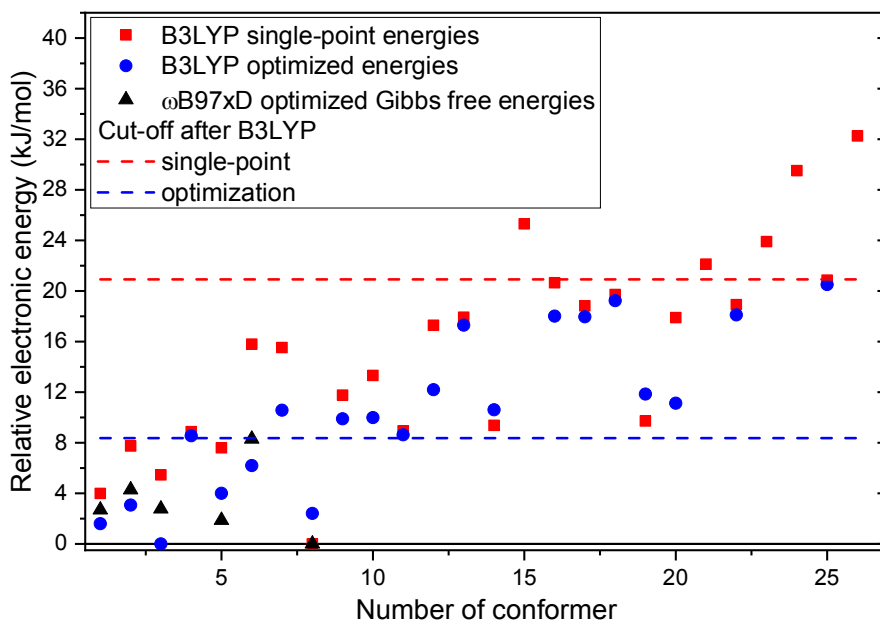


Figure 6 – An example of the conformer energies after each calculation step. The conformers under the cut-off lines were kept for the next calculations. The conformers are ordered based on their MMFF electronic energies. This molecule is one of the sample molecules of **Article III**, ((2R,3S)-oxirane-2,3-diyl)dimethanol.



## 2.2.1 Hydrogen bonded complexes

In ion-molecule clusters, a neutral molecule and an ion are bound by at least one hydrogen bond. If the ion is negatively charged, the hydrogen bond acceptor is a negatively charged atom in the anion, for instance, an oxygen or a halogen atom. The hydrogen bond donating groups in the neutral molecule can be a hydrogen atom or, for instance, a hydroxy, a hydroperoxy, a carboxylic acid, or a peroxy acid group. With positively charged ions, the cation acts as a hydrogen bond donor and the hydrogen bond acceptors are electronegative atoms of the neutral molecule.

The force field used for conformer sampling in Spartan '14, MMFF, can recognize an attractive interaction between hydrogen bond donors and acceptors in the ion-molecule clusters, especially when the hydrogen bond donating groups are hydroxy or hydroperoxy groups. Performing a systematic conformer sampling similar to the one for free molecules but with an additional reagent ion binding with the neutral molecule in the initial structure, gives a reasonable set of cluster conformers. There are, however, two reagent ions that were used in this work, where the MMFF force field does not work ideally:  $\text{CF}_3\text{O}^-$  and  $\text{I}^-$ . The fluorine atoms in the  $\text{CF}_3\text{O}^-$  ion tend to form hydrogen bonds to the neutral sample molecule. The relative energies of the higher level DFT calculations indicate that these bonds are weaker than the hydrogen bonds between the oxygen atom of  $\text{CF}_3\text{O}^-$  and the hydrogen bond donating groups of the sample molecule, as none of the low energy clusters contain hydrogen bonding of the fluorine atoms. In addition, the MMFF force field is not parametrized for iodine. Therefore, the conformer sampling with  $\text{I}^-$  is unable to find any cluster conformers. Replacing  $\text{I}^-$  with  $\text{Br}^-$  in the conformer sampling produces cluster geometries similar to the ones  $\text{I}^-$  would form. The  $\text{Br}^-$  cluster conformers were thus used to find the lowest energy  $\text{I}^-$  cluster.

The hydrogen bonding clusters are less flexible than the free molecules, especially in cases where there are two hydrogen bonding functional groups at different ends of a carbon chain that can form bonds to the reagent ion. This leads to larger, even  $> 5$  kJ/mol, energy differences between the two lowest-energy conformers. If the lowest energy cluster conformer is not found, the error is larger than if the lowest energy conformer of the free molecule is missed.

## 2.3 Clustering simulations

In **Article I**, the chemical ionization in the IMR region of a CIMS instrument was modelled using the Atmospheric Cluster Dynamics Code (ACDC<sup>96</sup>). The program models the formation ( $\beta$ , arrows pointing towards right in Figure 7) and evaporation ( $\gamma$ , arrows pointing towards left in Figure 7) of ion-molecule clusters using parameters from quantum chemistry. The time evolution ( $\frac{dc_i}{dt}$ ) of the concentration ( $c_i$ ) of a cluster  $i$  is calculated using the birth-death equations:

$$\frac{dc_i}{dt} = \frac{1}{2} \sum_{j < i} \beta_{j,(i-j)} c_j c_{(i-j)} + \sum_j \gamma_{(i+j) \rightarrow i} c_{i+j} - \sum_j \beta_{i,j} c_i c_j - \frac{1}{2} \sum_{j < i} \gamma_{i \rightarrow j} c_i + Q_i - S_i \quad (15)$$

In a CIMS instrument, the source term  $Q_i$  represents the initial concentrations of the molecules and the constant production of the ion, and the loss term  $S_i$  can include wall-losses and coagulation.

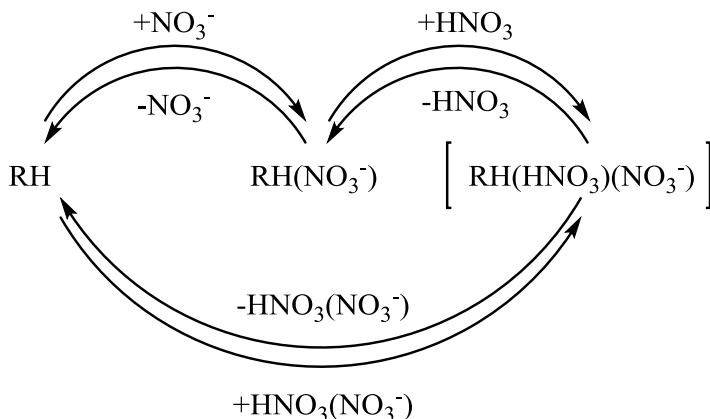


Figure 7 – Collisions and evaporations between a neutral sample molecule (RH),  $\text{NO}_3^-$  and  $\text{HNO}_3$ , modelled in ACDC.

The ACDC program uses kinetic gas theory to calculate the collision rates ( $\beta$ ) between neutral molecules and clusters using the masses ( $m$ ) and volumes ( $V$ , computed using the Gaussian 09 program<sup>97</sup>) of the molecules and clusters:

$$\beta_{ij} = \left(\frac{3}{4\pi}\right)^{1/6} \left(\frac{6k_bT}{m_i} + \frac{6k_bT}{m_j}\right)^{1/2} (V_i^{1/3} + V_j^{1/3})^2 \quad (16)$$

For the ion-neutral collisions, the Langevin collision rate:

$$\beta_{i,j}^{(L)} = q_i m_{red}^{-1/2} \left( \frac{\pi \alpha_j}{\epsilon_0} \right)^{1/2} \quad (17)$$

is used to calculate the final collision rates using the parametrization proposed by Su and Chesnavich:<sup>98</sup>

$$\beta_{i,j} = \begin{cases} \beta_{i,j}^{(L)} * (0.4767x + 0.6200), & x \geq 2 \\ \beta_{i,j}^{(L)} * \left( \frac{(x + 0.5090)^2}{10.526} + 0.9754 \right), & x < 2 \end{cases} \quad (18)$$

In Equation (17),  $q_i$  is the charge of the ion,  $m_{red}$  is the reduced mass of the colliding molecules/clusters,  $\alpha_j$  is the polarizability of the neutral molecule and  $\epsilon_0$  is the vacuum permittivity, and in Equation (18)

$$x = \frac{\mu_j}{(8\pi\epsilon_0\alpha_j k_B T)^{1/2}}, \quad (19)$$

where  $\mu_j$  is the dipole moment of the neutral molecule. In the simulation, all collisions are assumed to lead to cluster formation without an energy barrier, and the formed cluster is assumed to be collisionally stabilized by collisions with the bath gas.

The evaporation rates in the simulation are calculated using the detailed balance and assuming that the evaporation does not depend on the composition or pressure of the surrounding vapour. The evaporation rate of a cluster  $i + j$  into clusters  $i$  and  $j$  is calculated using the collision rate  $\beta_{i,j}$  and the formation free energies ( $\Delta G$ ) of clusters  $i$ ,  $j$  and  $i + j$ .

$$\gamma_{i,j} = \frac{p}{k_B T} \beta_{i,j} \exp\left(\frac{\Delta G_{i+j} - \Delta G_i - \Delta G_j}{k_B T}\right), \quad (20)$$

where  $p$  is the pressure.

The free energy of the  $\text{HNO}_3 - \text{NO}_3^-$  - sample molecule cluster in square brackets in Figure 7 was calculated only for one sample molecule in **Article I**, the  $\text{C}_6\text{H}_8\text{O}_7$  product from cyclohexene ozonolysis. In the simulation, the concentration of the cluster was low, so the equivalent clusters of the other sample molecules were not included in the model. Instead, if a sample molecule collides with a reagent ion cluster (in this case an  $\text{HNO}_3(\text{NO}_3^-)$  cluster) the probabilities of each evaporation pathway were calculated from the formation free energies of the reagent ion cluster and the ion-molecule cluster.

In the ACDC simulation in **Article I**, the reagent ion distribution was first generated by mixing a constant number concentration of  $\text{NO}_3^-$  with  $\text{HNO}_3$ . The formed reagent ions can contain either zero, one or two neutral  $\text{HNO}_3$  molecules. After the reagent ion distribution was created, a second simulation mixed the negatively charged reagent ions and clusters with the neutral sample molecules to simulate the charging of the sample molecules in the IMR region of the instrument. In the instrument, the reagent ions are introduced to the sample flow in the IMR region using an electric field, but due to diffusion and turbulent air flow, a fraction of the neutral  $\text{HNO}_3$  is mixed to the sample reagent flow. This makes it difficult to estimate the  $\text{HNO}_3$  concentration in the mixture. For this reason, we tested adding different concentrations of  $\text{HNO}_3$  to the second part of the simulation. In addition, two different  $\text{HNO}_3$  concentrations in the first part of the simulation were tested to see the effect of different types of reagent ion distributions on the ionization.

## 2.4 Reaction rate coefficients

Reaction rate coefficients ( $k$ ) of unimolecular reactions are commonly calculated using various forms of transition state theory (TST). The simple form of TST includes one reactant and one transition state:

$$k_{TST} = \kappa \frac{k_b T}{h} \frac{Q_{TST}}{Q_R} \exp\left(-\frac{E_{TST} - E_R}{k_b T}\right), \quad (21)$$

where  $\kappa$  is a tunnelling factor. The potential energy barrier between the reactant and the product ( $E_{TST} - E_R$ ) and the partition functions of the reactant and transition state ( $Q_R$  and  $Q_{TST}$  respectively) can be calculated with quantum chemical methods. Here, it is important to have an accurate potential energy barrier because even small errors in the exponent lead to large errors in the reaction rate. The tunnelling factor is commonly calculated using one dimensional factors, such as the Wigner correction or Eckart<sup>99</sup> tunnelling correction. In small systems, tunnelling can be included by using, for instance, the harmonic quantum transition state theory (HQTST<sup>100</sup>), where the instanton theory is used to calculate the reaction rate and the tunnelling factor can be calculated from the difference between the TST and HQTST reaction rates. Other reaction rate calculation methods include, for

instance, variational TST<sup>101</sup> and long-range TST.<sup>102</sup> These can be used in bimolecular reaction rate calculations especially when the reaction has no clear transition state.

There are different ways of selecting the conformers that are used in a TST calculation. It has been recently shown in **Article VII**, using an H-shift reaction of a small model system, that employing the most accurate calculations available and including all of the low energy conformers until a certain limit, will give the slowest reaction rate compared to using calculations at a lower level of theory and using only one set of conformers in the calculations. This observation will help in ruling out the slowest reaction rates, for instance, in the atmospheric oxidation of VOCs. If a reaction rate calculated using only the lowest energy conformers of the reactant and transition state is too low to play a role in the atmosphere, it is likely too low also after multiple conformers are added to the calculation.

In **Article IV**, the reaction rate coefficients of the unimolecular HO<sub>2</sub> loss reaction, proposed to terminate the autoxidation reaction chain, were calculated under atmospheric conditions using TST. As the O<sub>2</sub> addition reaction to alkyl radicals (forming the reactant of the studied reaction) is generally exothermic, we also tested the effect of excess energy to the reaction by using the Master Equation Solver for Multi-Energy well Reactions (MESMER<sup>103</sup>) program. The MESMER program calculates the reaction rate coefficients using the Rice-Ramsperger-Kassel-Marcus (RRKM) theory, which is a more appropriate approach than TST in cases where the intermediate species are not collisionally stabilized. The program can take into account the excess energy in multi-well reactions, which is not possible using TST. As input, MESMER uses the vibrational frequencies and energies calculated using quantum chemistry. Additional collision parameters, such as Lennard-Jones parameters, are used to simulate the collisional stabilization.

## 3 RESULTS

### 3.1 Lowest free energy cluster conformers

In anion chemical ionization, the reagent ion forms one or more hydrogen bonds to the hydrogen bond donating functional groups of the neutral sample molecule. Commonly in oxidized organic molecules, the hydrogen bond donating groups are the hydrogens of hydroxy, hydroperoxy groups, or carboxylic or peroxy acid groups. The most stable ion-molecule clusters have one or two hydrogen bond donating groups binding with the reagent ion, even if the sample molecule contains more than two hydrogen bond donating functional groups. This has been seen in calculations on  $\text{NO}_3^-$ ,  $\text{CH}_3\text{C}(\text{O})\text{O}^-$ ,  $\text{CH}_3\text{CH}(\text{OH})\text{C}(\text{O})\text{O}^-$ , trifluoroacetate ( $\text{CF}_3\text{C}(\text{O})\text{O}^-$ ), trifluoromethanolate ( $\text{CF}_3\text{O}^-$ ), bromide ( $\text{Br}^-$ ) and iodide ( $\text{I}^-$ ) clusters in **Articles I-III**. The additional functional groups increase the stability of the cluster by polarizing the functional groups that are binding with the ion. In some instances, the reagent ion also has two or more hydrogen bonding functional groups, such as  $\text{NO}_3^-$ ,  $\text{CH}_3\text{C}(\text{O})\text{O}^-$  and  $\text{CH}_3\text{CH}(\text{OH})\text{C}(\text{O})\text{O}^-$ . In these reagent ions, the charge is divided between two oxygen atoms. Generally, the cluster conformer is more stable if both of those atoms are binding with one of the hydrogen bond donating groups of the sample molecule.

In **Articles II and III**, we found that the lowest free energy ion-molecule cluster conformers are, for most sample molecules, the same with all of the reagent anions. This information can be used in the conformer sampling if clusters with different reagent ions are computed simultaneously. Figure 8 illustrates the similarity of the sample molecule geometries clustered with a)  $\text{CH}_3\text{C}(\text{O})\text{O}^-$ , b)  $\text{NO}_3^-$ , c)  $\text{I}^-$  and d)  $\text{CF}_3\text{O}^-$ .

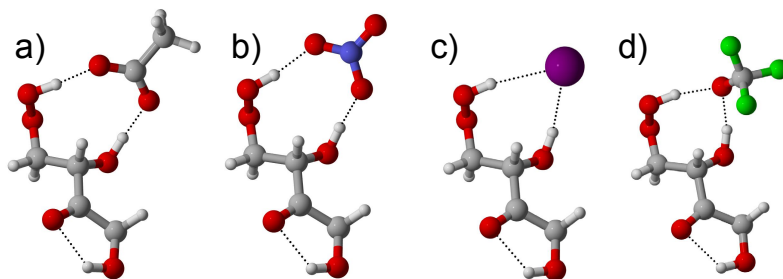


Figure 8 – The lowest free energy conformers of  $C_4H_8O_5$  clustered with a)  $CH_3C(O)O^-$ , b)  $NO_3^-$ , c)  $I^-$ , and  $CF_3O^-$ . Color coding: grey = C, red = O, white = H, blue = N, purple = I, green = F.

### 3.2 Formation free energies

The formation free energies of  $NO_3^-$  and  $CH_3C(O)O^-$  clusters have been calculated for several sample molecules that contain two or more hydrogen bond donating functional groups and varying number of oxygen atoms:

- OH-initiated oxidation products of butadiene (as a surrogate for isoprene) containing between two and six oxygen atoms (from **Article III**) and one OH-initiated oxidation product of isoprene (isoprene epoxydiol, IEPOX). The hydrogen bonding functional groups in these compounds are hydroxy and hydroperoxy groups.
- $RO_2$  radical intermediates and closed-shell products of  $O_3$ -initiated autoxidation of cyclohexene (from **Articles I and II**) that contain carbonyl, hydroperoxy and peroxy acid groups.
- Model  $RO_2$  radical compounds (from **Article V**) that contain a peroxy acid group and either a hydroxy or a hydroperoxy group.

The formation free energies of the  $NO_3^-$  and  $CH_3C(O)O^-$  clusters have been plotted in Figure 9. The energies were calculated at the  $\omega B97xD/aug-cc-pVTZ$  level of theory. The formation free energies of the ion-molecule clusters generally decrease, i.e., the stability of the cluster increases, when the number of oxygen atoms in the sample molecule increases.

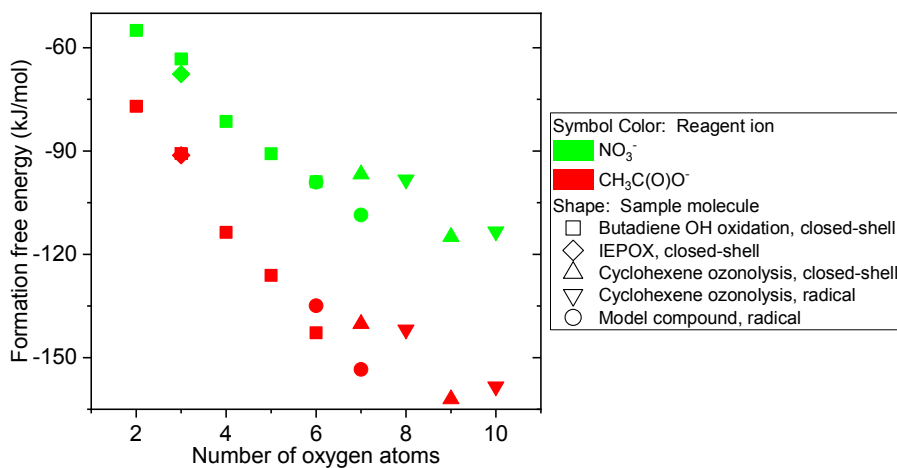


Figure 9 - Formation free energies of  $\text{NO}_3^-$  and  $\text{CH}_3\text{C}(\text{O})\text{O}^-$  clusters from three different studies, calculated at the  $\omega\text{B97xD/aug-cc-pVTZ}$  level of theory.

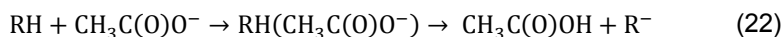
The closed-shell products of the OH-initiated oxidation of butadiene show a linear correlation between the number of oxygen atoms in the sample molecule and the formation free energy of the cluster. The other sample molecule types each only have one or two points, which makes it impossible to determine the correlation between the number of oxygen atoms and the formation free energy. The closed-shell products of cyclohexene ozonolysis could possibly have the same slope, but a different intercept, compared to the OH oxidation products. The strong intramolecular hydrogen bonding of the peroxy acid groups might lead to higher formation free energies than the OH oxidation products that do not contain acid groups. It is also likely that the formation free energy converges toward some limiting energy value as more oxygen atoms are added to the sample molecule.

It is noticed that the formation free energy does not significantly change going from 7 and 9 oxygen atom closed-shell products to 8 and 10 oxygen atom  $\text{RO}_2$  radical intermediates of cyclohexene oxidation, respectively. Presumably the radical oxygen atom in the peroxy radical group is unable to polarize the sample molecule as effectively as non-radical oxygen atoms, since in all other cases in Figure 9 the addition of an oxygen atom would decrease the formation free energy of the cluster.



### 3.3 Deprotonation

In some CIMS instruments, the sample molecules are ionized by proton transfer. Especially  $\text{CH}_3\text{C}(\text{O})\text{O}^-$  is often used as a reagent ion to deprotonate various sample molecules (RH). The deprotonation energy can be calculated as the energy of the reaction:



However,  $\text{CH}_3\text{C}(\text{O})\text{O}^-$  is also able to form stable clusters with the sample molecules. This cluster is on the reaction path of the deprotonation reaction, i.e., the clustering needs to take place before deprotonation can occur. The deprotonation reaction is thus a two-step process where the first step forms an intermediate cluster and the second step fragments the cluster into the products, deprotonated sample molecule ( $\text{R}^-$ ) and  $\text{CH}_3\text{C}(\text{O})\text{OH}$ .

Figure 10 shows an example of the free energies of the reactants and the products of deprotonation with  $\text{CH}_3\text{C}(\text{O})\text{O}^-$  relative to the  $\text{CH}_3\text{C}(\text{O})\text{O}^-$  clusters. The sample molecules are OH-initiated oxidation products of butadiene with a different number of oxygen atoms. On the left hand side in Figure 10, there are the free energies of the reactants (the sample molecule and reagent ion) relative to the cluster energy. On the right hand side, there are the energies of the deprotonation products relative to the cluster.

In some CIMS instruments, the clusters are fragmented intentionally, for instance, using a CDC, to detect only sample molecules that can be deprotonated by  $\text{CH}_3\text{C}(\text{O})\text{O}^-$ . The clusters can also fragment unintentionally due to voltage changes and high energy collisions inside the mass spectrometer. If the formed clusters are fragmented, Figure 10 can give an indication on how the cluster fragments. The cluster is more likely to break apart towards the lower energy fragments (reactants or products). For the more oxidized sample molecule in Figure 10 ( $\text{C}_4\text{H}_{10}\text{O}_4$ ,  $\text{C}_4\text{H}_8\text{O}_5$  and  $\text{C}_4\text{H}_{10}\text{O}_6$ ), the more probable fragmentation pathway is deprotonation whereas for the least oxidized molecule ( $\text{C}_4\text{H}_8\text{O}_3$ ), fragmentation back to the reactants is more favourable.

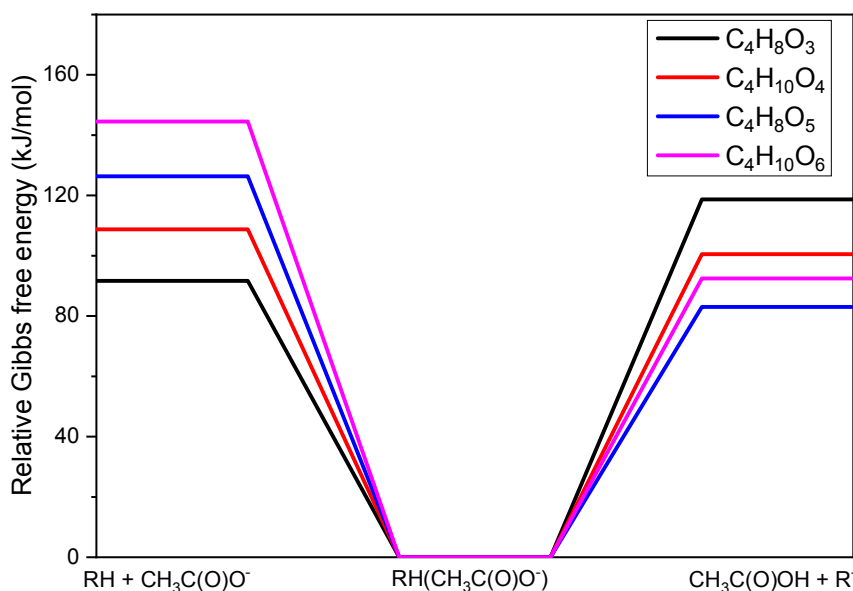


Figure 10 – The free energies of the reactants (the neutral sample molecule and  $\text{CH}_3\text{C}(\text{O})\text{O}^-$ ) on the left hand side and products (the deprotonated sample molecule and  $\text{CH}_3\text{C}(\text{O})\text{OH}$ ) on the right hand side, relative to the  $\text{CH}_3\text{C}(\text{O})\text{O}^-$  cluster. The energies are calculated at the DLPNO-CCSD(T)/def2-QZVPP// $\omega$ B97xD/aug-cc-pVTZ level of theory.

In CIMS measurements, the sample molecules discussed are still not necessarily detected as deprotonation products. If the CIMS instrument does not have a CDC, the energy difference between the cluster and the fragmentation products also needs to be low enough for the stable cluster to fragment. Otherwise, only the clusters are detected. Deprotonation energies were calculated in **Article II** and **Article III**. Generally the energy difference between the  $\text{CH}_3\text{C}(\text{O})\text{O}^-$  cluster and the deprotonation products is smaller for the peroxy acid containing sample molecules derived from an ozonolysis reaction than for the sample molecules that contain hydroxy and hydroperoxy groups.

### 3.4 Fluoride transfer

Fluoride transfer reaction is common in measurements using  $\text{CF}_3\text{O}^-$  as a reagent ion. Fluoride transfer products are mainly detected in chemical ionization of small

sample molecules. In a fluoride transfer reaction, one of the fluorine atoms of the  $\text{CF}_3\text{O}^-$  reagent ion is transferred to the sample molecule forming an  $\text{F}^-$  cluster:

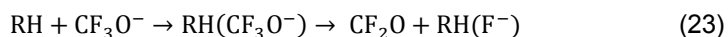


Figure 11 show the energetics of the fluoride transfer similar to Figure 10 for deprotonation with  $\text{CH}_3\text{C}(\text{O})\text{O}^-$ . The  $\text{CF}_3\text{O}^-$  clusters are significantly less stable than the  $\text{CH}_3\text{C}(\text{O})\text{O}^-$  clusters of these sample molecules. Thus, the energy difference between the cluster and the fluoride transfer products (fluorinated sample molecule and  $\text{CF}_2\text{O}$ ) is smaller. The fluoride transfer reaction would be favourable for all of the four sample molecules in Figure 11.

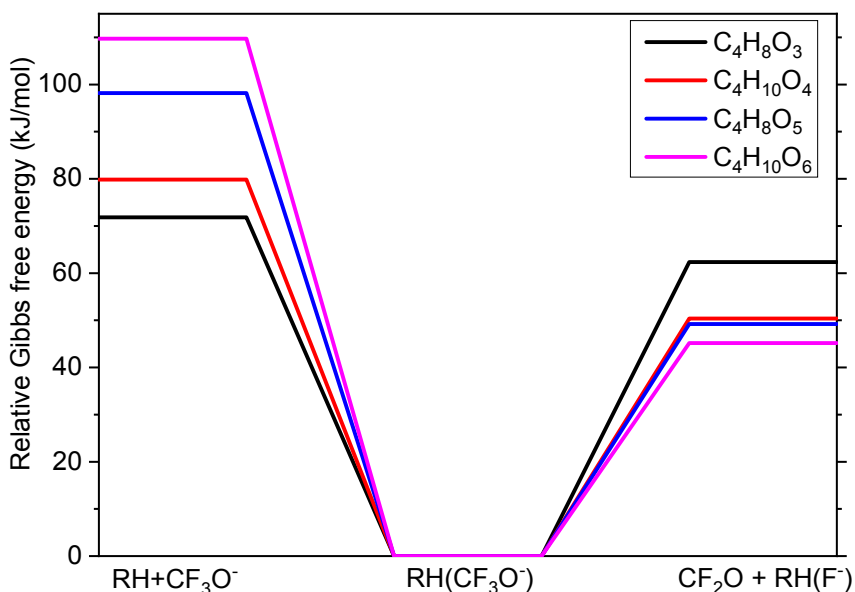


Figure 11 – The free energies of the reactants (neutral sample molecule and  $\text{CF}_3\text{O}^-$ ) on the left and products (fluorinated sample molecule and  $\text{CF}_2\text{O}$ ) on the right, relative to the  $\text{CF}_3\text{O}^-$  cluster. The energies are calculated at the DLPNO-CCSD(T)/def2-QZVPP// $\omega$ B97xD/aug-cc-pVTZ level of theory.

In **Article III**, the fluoride transfer reaction was calculated for the OH-initiated oxidation products of butadiene. The more favourable fragmentation pathway of the  $\text{CF}_3\text{O}^-$  clusters, for all of the calculated sample molecules, was found to be the fluoride transfer, as opposed to the fragmentation back to the sample molecule and reagent ion.

### 3.5 Unimolecular HO<sub>2</sub> loss

The unimolecular HO<sub>2</sub> loss reaction has been suggested to terminate the radical reaction chain in the autoxidation of VOCs in order to explain the formation of a closed-shell product that has an even number of oxygen atoms.<sup>39</sup> The formation of products from the ozonolysis of endocyclic alkenes containing an odd number of oxygen atoms was explained by a unimolecular OH loss reaction. Both types of products were measured in laboratory experiments using an NO<sub>3</sub><sup>-</sup> chemical ionization. A concerted HO<sub>2</sub> loss reaction has been measured with small amines under atmospheric conditions,<sup>104</sup> but not with hydrocarbons.<sup>105</sup>

Figure 12 shows two different pathways for a unimolecular HO<sub>2</sub> loss: a concerted (above) and a two-step (below) reaction. The concerted reaction contains one transition state (TS) where simultaneously the C-O and C-H bonds are broken and the O-H bond and the C-C double bond are formed. The two-step reaction includes one transition state for the H-shift reaction and another transition state for the breaking of the C-O bond.

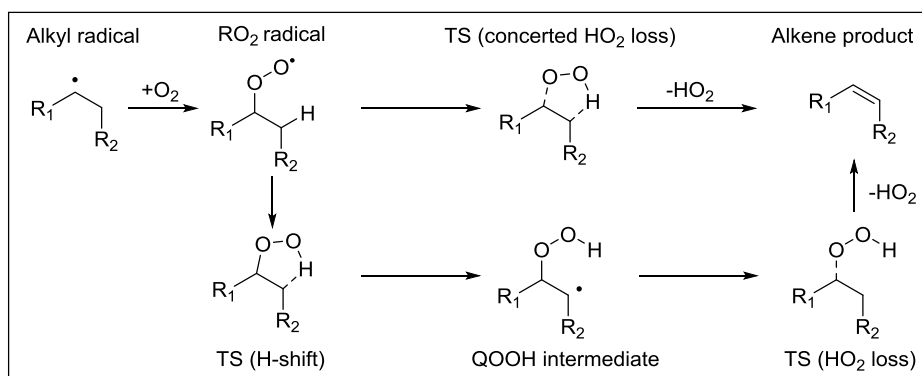


Figure 12 - The two mechanisms of a unimolecular HO<sub>2</sub> loss reaction.

The energetics of both reaction paths were calculated in **Article IV** for molecules where R<sub>1</sub> and R<sub>2</sub> are either a methyl group (-CH<sub>3</sub>) or a peroxy acid group. The energy barrier of the concerted HO<sub>2</sub> loss is, for all four reactants, lower than the H-shift barrier in the two-step reaction pathway. Even with the lower potential energy barrier of the concerted HO<sub>2</sub> loss mechanism, the reaction rate is too slow

compared to the rates of competing bimolecular reactions (with molecules such as HO<sub>2</sub>, NO<sub>2</sub> and NO) under atmospheric conditions.

Generally, reactions with high energy barriers are slow. In autoxidation reactions, the exothermic O<sub>2</sub> addition reaction forms an intermediate RO<sub>2</sub> radical that has excess energy. If the molecule is small enough, it can react further before the intermediate is collisionally stabilized. This means that even unimolecular reactions with high energy barriers can be fast. However, larger organic molecules have so many vibrational modes that the formed molecule is likely collisionally stabilized before it reacts further. Already simple methyl groups in the places of R<sub>1</sub> and R<sub>2</sub> lead to complete collisional stabilization of the RO<sub>2</sub> radical under atmospheric pressures. This was seen in the MESMER simulations of the HO<sub>2</sub> loss reactions in **Article IV**. Decreasing the pressure in the MESMER calculations showed that the total reaction shown in Figure 12 is much faster without collisional stabilization caused by collisions with the bath gas. In conditions where the intermediate is almost completely collisionally stabilized, MESMER calculates reaction rate coefficients close to the TST rates.

## 4 SUMMARY AND CONCLUSIONS OF THE INDIVIDUAL RESEARCH ARTICLES

### 4.1 Article I: Cluster stabilities with $\text{NO}_3^-$

Closed-shell products of cyclohexene ozonolysis and autoxidation have been measured using  $\text{NO}_3^-$  chemical ionization. The CIMS instrument was able to detect highly oxidized products with 7-9 oxygen atoms.<sup>39</sup> In **Article I**, we calculated the formation free energies of the ion-molecule clusters of these proposed chemical structures, and one less oxidized product with 5 oxygen atoms. These energies were then used in clustering simulations to model the chemical ionization processes in the IMR region of a CIMS instrument.

With the calculations, we were able to explain why the least oxidized autoxidation product (with 5 oxygen atoms) was not detected in the experiments. In addition, we found that the formation free energy of the proposed structure for the product with 8 oxygen atoms is too high for the molecule to be detected efficiently. We concluded that the structure of the detected species likely differs from the one that was proposed by Rissanen et al.<sup>39</sup>

### 4.2 Article II: Cluster stabilities with $\text{NO}_3^-$ and $\text{CH}_3\text{C}(\text{O})\text{O}^-$

In a subsequent experimental study by Berndt et al.,<sup>69</sup> the closed-shell products and  $\text{RO}_2$  intermediates of cyclohexene ozonolysis were measured using two different reagent ions:  $\text{NO}_3^-$  and  $\text{CH}_3\text{C}(\text{O})\text{O}^-$ . The study indicated that  $\text{CH}_3\text{C}(\text{O})\text{O}^-$  has a higher detection efficiency than  $\text{NO}_3^-$  when measuring less oxidized sample molecules, and that a significant fraction of some sample molecules is deprotonated by  $\text{CH}_3\text{C}(\text{O})\text{O}^-$ .

In **Article II**, we computed formation free energies of the  $\text{NO}_3^-$  and  $\text{CH}_3\text{C}(\text{O})\text{O}^-$  clusters of the  $\text{RO}_2$  intermediates and closed-shell products (see Table 1). The  $\text{CH}_3\text{C}(\text{O})\text{O}^-$  clusters were found to be significantly more stable than the  $\text{NO}_3^-$  clusters.

Table 1 - Formation free energies and enthalpies of the  $\text{NO}_3^-$  and  $\text{CH}_3\text{C}(\text{O})\text{O}^-$  clusters in kJ/mol (kcal/mol). The energies are calculated at the  $\omega\text{B97xD/aug-cc-pVTZ}$  level of theory at 298.15 K and 1 atm reference pressure.

	$\Delta\text{G}$		$\Delta\text{H}$	
	$\text{NO}_3^-$	$\text{CH}_3\text{C}(\text{O})\text{O}^-$	$\text{NO}_3^-$	$\text{CH}_3\text{C}(\text{O})\text{O}^-$
$\text{C}_6\text{H}_8\text{O}_5$	-71.42 (-17.07)	-101.13 (-24.17)	-123.64 (-29.55)	-160.79 (-38.43)
$\text{C}_6\text{H}_9\text{O}_6$	-77.78 (-18.59)	-111.04 (-26.54)	-128.62 (-30.74)	-169.08 (-40.41)
$\text{C}_6\text{H}_8\text{O}_7$	-96.73 (-23.12)	-140.21 (-33.51)	-146.77 (-35.08)	-201.42 (-48.14)
$\text{C}_6\text{H}_9\text{O}_8$	-98.28 (-23.49)	-141.88 (-33.91)	-149.83 (-35.81)	-203.47 (-48.63)
$\text{C}_6\text{H}_8\text{O}_9$	-114.89 (-27.46)	-162.00 (-38.72)	-163.39 (-39.05)	-220.16 (-52.62)
$\text{C}_6\text{H}_9\text{O}_{10}$	-113.34 (-27.09)	-158.36 (-37.85)	-166.65 (-39.83)	-225.10 (-53.80)

In addition, we computed the energies of the deprotonated sample molecules in order to explain computationally, why  $\text{CH}_3\text{C}(\text{O})\text{O}^-$  is able to deprotonate some of the sample molecules and  $\text{NO}_3^-$  is not. The free energies of clustering, deprotonation, and other chemical ionization reactions of the  $\text{C}_6\text{H}_8\text{O}_7$  sample molecule are shown in Table 2, with additional cluster formation energies in the presence of hydrated reagent ions that were computed in **Article III**.

Table 2 – Reaction free energies of the C<sub>6</sub>H<sub>8</sub>O<sub>7</sub> product from cyclohexene ozonolysis at 298.15 K and 1 atm reference pressure, calculated at the DLPNO-CCSD(T)/def2-QZVPP// $\omega$ B97xD/aug-cc-pVTZ level of theory.

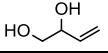
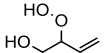
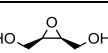
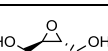
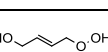
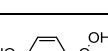
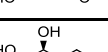
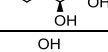
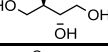
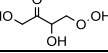
	kJ/mol		kcal/mol	
	NO <sub>3</sub> <sup>-</sup>	CH <sub>3</sub> C(O)O <sup>-</sup>	NO <sub>3</sub> <sup>-</sup>	CH <sub>3</sub> C(O)O <sup>-</sup>
QH + Q <sup>-</sup> → QH(Q <sup>-</sup> )	-89.78	-72.96	-21.46	-17.44
RH + Q <sup>-</sup> → RH(Q <sup>-</sup> )	-100.03	-139.05	-23.91	-33.23
RH + QH(Q <sup>-</sup> ) → QH + RH(Q <sup>-</sup> )	-10.25	-66.09	-2.45	-15.80
RH(Q <sup>-</sup> ) → QH + R <sup>-</sup>	105.02	53.85	25.10	12.87
H <sub>2</sub> O + Q <sup>-</sup> → H <sub>2</sub> O(Q <sup>-</sup> )	-31.01	-38.25	-7.41	-9.14
H <sub>2</sub> O + QH(Q <sup>-</sup> ) → QH + H <sub>2</sub> O(Q <sup>-</sup> )	58.77	34.70	14.05	8.29
RH + H <sub>2</sub> O(Q <sup>-</sup> ) → H <sub>2</sub> O + RH(Q <sup>-</sup> )	-69.01	-100.79	-16.49	-24.09
RH + (H <sub>2</sub> O) <sub>2</sub> (Q <sup>-</sup> ) → 2H <sub>2</sub> O + RH(Q <sup>-</sup> )	-52.54	-81.29	-12.56	-19.43
RH + (H <sub>2</sub> O) <sub>3</sub> (Q <sup>-</sup> ) → 3H <sub>2</sub> O + RH(Q <sup>-</sup> )	-45.08	-60.25	-10.77	-14.40

### 4.3 Article III: Chemical ionization with different reagent ions

In **Article III**, we investigated chemical ionization more extensively using different reagent anions and a larger set of smaller sample molecules. A summary of the formation enthalpies of the ion-molecule clusters is given in Table 3. The effect of water on detection efficiencies was also investigated by calculating the stabilities of hydrated reagent ions and ion-molecule clusters. We found that the formation free energies of the ion-molecule clusters correlate with the number of oxygen atoms in the sample molecule, rather than the number of hydrogen bond donating functional groups in the molecule.



Table 3 - The formation enthalpies of the ion-molecule clusters of OH-initiated oxidation products of isoprene and different reagent anions, calculated at the DLPNO-CCSD(T)/def2-QZVPP// $\omega$ B97xD/aug-cc-pVTZ level of theory.

	NO <sub>3</sub> <sup>-</sup>	CH <sub>3</sub> C(O)O <sup>-</sup>	CH <sub>3</sub> CH(OH) C(O)O <sup>-</sup>	CF <sub>3</sub> C(O)O <sup>-</sup>	CF <sub>3</sub> O <sup>-</sup>	Br <sup>-</sup>	I <sup>-</sup>
	-97.45 (-23.29)	-125.48 (-29.99)	-109.29 (-26.12)	-97.91 (-23.40)	-98.11 (-23.45)	-96.90 (-23.16)	-75.14 (-17.96)
	-106.44 (-25.44)	-137.90 (-32.96)	-120.62 (-28.83)	-111.13 (-26.56)	-110.21 (-26.34)	-110.08 (-26.31)	-87.45 (-20.90)
	-114.52 (-27.37)	-144.60 (-34.56)	-126.40 (-30.21)	-114.68 (-27.41)	-123.26 (-29.46)	-122.72 (-29.33)	-100.12 (-23.93)
	-103.14 (-24.65)	-134.10 (-32.05)	-115.19 (-27.53)	-103.30 (-24.69)	-104.18 (-24.90)	-107.32 (-25.65)	-84.81 (-20.27)
	-119.03 (-28.45)	-142.76 (-34.12)	-127.36 (-30.44)	-116.27 (-27.79)	-117.36 (-28.05)	-116.40 (-27.82)	-95.35 (-22.79)
	-102.55 (-24.51)	-137.74 (-32.92)	-117.78 (-28.15)	-106.61 (-25.48)	-108.28 (-25.88)	-108.74 (-25.99)	-86.57 (-20.69)
	-117.78 (-28.15)	-155.48 (-37.16)	-135.90 (-32.48)	-122.76 (-29.34)	-118.83 (-28.40)	-122.51 (-29.28)	-99.12 (-23.69)
	-128.24 (-30.65)	-165.73 (-39.61)	-145.90 (-34.87)	-132.97 (-31.78)	-130.62 (-31.22)	-133.22 (-31.84)	-109.75 (-26.23)
	-135.73 (-32.44)	-176.90 (-42.28)	-156.02 (-37.29)	-142.88 (-34.15)	-143.85 (-34.38)	-143.68 (-34.34)	-119.24 (-28.50)
	-148.20 (-35.42)	-193.97 (-46.36)	-170.75 (-40.81)	-156.36 (-37.37)	-154.98 (-37.04)	-158.24 (-37.82)	-132.84 (-31.75)

#### 4.4 Article IV: Concerted HO<sub>2</sub> loss in autoxidation reactions

Based on the results of **Article I**, we took a closer look at the unimolecular HO<sub>2</sub> loss reaction, proposed by Rissanen et al.,<sup>39</sup> that forms a closed-shell product with an even number of oxygen atoms in the ozonolysis of cyclohexene. In **Article IV**, the reaction rate coefficients of two different unimolecular HO<sub>2</sub> loss reaction mechanisms were calculated for four model compounds. We found that the HO<sub>2</sub> loss reaction from hydrocarbons is slow under atmospheric conditions, even with the excess energy from the O<sub>2</sub> addition reaction. This conclusion is in line with the result of **Article I** that the structure of the measured C<sub>6</sub>H<sub>8</sub>O<sub>8</sub> molecule is likely not a product of unimolecular HO<sub>2</sub> loss.

## Computational tools: a review of the used software

**Spartan '14**<sup>89</sup> is a quantum chemical program and was used for the (systematic) conformer sampling using the MMFF method and DFT calculations, both single-point and geometry optimization, using the B3LYP/6-31+G\* level of theory.

**Gaussian 09, Revisions C.01 and D.01**<sup>97</sup> are program suites for electronic structure calculations. In this work, Gaussian 09 was used for density functional theory (DFT) calculations in all of the articles using the B3LYP/6-31+G\* and  $\omega$ B97xD/aug-cc-pVTZ levels of theory to optimize geometries and calculate the vibrational frequencies of all molecules and clusters.

**ORCA**<sup>106</sup> **versions 3.0.1 and 3.0.3** were used to calculate the coupled cluster single-point energies of the closed-shell species in **Articles I, II and III** using mainly the DLPNO-CCSD(T) /def2-QZVPP level of theory.

**Molpro versions 2012.1**<sup>107,108</sup> and **2015.1**<sup>107,109</sup> were used in this thesis to calculate the single-point energies at the ROHF-ROCCSD(T)-F12a/VDZ-F12 level of theory in **Articles III and IV**.

Atmospheric Clustering Dynamics Code (**ACDC**<sup>96</sup>) is a program for calculating collision and evaporation rate coefficients and for simulating the clustering of molecules and ions in the gas-phase using these parameters. The program was used in **Article I** to simulate the chemical ionization of different sample molecule inside the CI-API-TOF instrument.

Master Equation Solver for Multi-Energy well Reactions (**MESMER**<sup>103</sup>) is a reaction kinetics program for calculating Bartis-Widom reaction rate coefficients for different types of unimolecular and bimolecular reactions. The program was used in **Article II** to test the collisional stabilization of the ion-molecule clusters in a chemical ionization measurements, and in **Article IV** to calculate the reaction rate coefficients of the unimolecular HO<sub>2</sub> loss reactions.

## REFERENCES

1. Stephens, E. R. Chemistry of atmospheric oxidants. *Journal of the Air Pollution Control Association* **1969**, *19*, 181-185.
2. Kesselmeier, J.; Staudt, M. Biogenic volatile organic compounds (VOC): An overview on emission, physiology and ecology. *Journal of Atmospheric Chemistry* **1999**, *33*, 23-88.
3. Kansal, A. Sources and reactivity of NMHCs and VOCs in the atmosphere: A review. *Journal of Hazardous Materials* **2009**, *166*, 17-26.
4. Kroll, J. H.; Seinfeld, J. H. Chemistry of secondary organic aerosol: Formation and evolution of low-volatility organics in the atmosphere. *Atmospheric Environment* **2008**, *42*, 3593-3624.
5. Holloway, A. M.; Wayne, R. P. *Atmospheric Chemistry*; Royal Society of Chemistry: Cambridge, UK, 2010; pp 99-115.
6. Warneke, C.; de Gouw, J. A.; Goldan, P. D.; Kuster, W. C.; Williams, E. J.; Lerner, B. M.; Jakoubek, R.; Brown, S. S.; Stark, H.; Aldener, M.; Ravishankara, A. R.; Roberts, J. M.; Marchewka, M.; Bertman, S.; Sueper, D. T.; Mckeen, S. A.; Meagher, J. F.; Fehsenfeld, F. C. Comparison of daytime and nighttime oxidation of biogenic and anthropogenic VOCs along the New England coast in summer during New England Air Quality Study 2002. *Journal of Geophysical Research: Atmospheres* **2004**, *109*, D10309.
7. Atkinson, R.; Arey, J. Atmospheric degradation of volatile organic compounds. *Chemical Reviews* **2003**, *103*, 4605-4638.
8. Atkinson, R. Atmospheric chemistry of VOCs and NO<sub>x</sub>. *Atmospheric Environment* **2000**, *34*, 2063-2101.
9. Atkinson, R.; Arey, J. Gas-phase tropospheric chemistry of biogenic volatile organic compounds: A review. *Atmospheric Environment* **2003**, *37*, 197-219.
10. Crouse, J. D.; Paulot, F.; Kjaergaard, H. G.; Wennberg, P. O. Peroxy radical isomerization in the oxidation of isoprene. *Physical Chemistry Chemical Physics* **2011**, *13*, 13607-13613.
11. Crouse, J. D.; Knap, H. C.; Ørnsø, K. B.; Jørgensen, S.; Paulot, F.; Kjaergaard, H. G.; Wennberg, P. O. Atmospheric fate of methacrolein. 1. Peroxy radical

- isomerization following addition of OH and O<sub>2</sub>. *The Journal of Physical Chemistry A* **2012**, *116*, 5756-5762.
12. Crouse, J. D.; Nielsen, L. B.; Jørgensen, S.; Kjaergaard, H. G.; Wennberg, P. O. Autoxidation of organic compounds in the atmosphere. *The Journal of Physical Chemistry Letters* **2013**, *4*, 3513-3520.
  13. Ehn, M.; Thornton, J. A.; Kleist, E.; Sipilä, M.; Junninen, H.; Pullinen, I.; Springer, M.; Rubach, F.; Tillmann, R.; Lee, B.; Lopez-Hilfiker, F.; Anders, S.; Acir, I.; Rissanen, M. P.; Jokinen, T.; Schobesberger, S.; Kangasluoma, J.; Kontkanen, J.; Nieminen, T.; Kurtén, T.; Nielsen, L. B.; Jørgensen, S.; Kjaergaard, H. G.; Canagaratna, M.; Dal Maso, M.; Berndt, T.; Petäjä, T.; Wahner, A.; Kerminen, V.; Kulmala, M.; Worsnop, D. R.; Wildt, J.; Mentel, T. F. A large source of low-volatility secondary organic aerosol. *Nature* **2014**, *506*, 476-479.
  14. Praske, E.; Otkjær, R. V.; Crouse, J. D.; Hethcox, J. C.; Stoltz, B. M.; Kjaergaard, H. G.; Wennberg, P. O. Atmospheric autoxidation is increasingly important in urban and suburban North America. *Proceedings of the National Academy of Sciences* **2018**, *115*, 64-69.
  15. Kurtén, T.; Tiusanen, K.; Roldin, P.; Rissanen, M.; Luy, J.; Boy, M.; Ehn, M.; Donahue, N.  $\alpha$ -pinene autoxidation products may not have extremely low saturation vapor pressures despite high O:C ratios. *The Journal of Physical Chemistry A* **2016**, *120*, 2569-2582.
  16. Weber, R. J.; Marti, J. J.; McMurry, P. H.; Eisele, F. L.; Tanner, D. J.; Jefferson, A. Measured atmospheric new particle formation rates: Implications for nucleation mechanisms. *Chemical Engineering Communications* **1996**, *151*, 53-64.
  17. Sihto, S.; Kulmala, M.; Kerminen, V.; Dal Maso, M.; Petäjä, T.; Riipinen, I.; Korhonen, H.; Arnold, F.; Janson, R.; Boy, M.; Laaksonen, A.; Lehtinen, K. E. J. Atmospheric sulphuric acid and aerosol formation: Implications from atmospheric measurements for nucleation and early growth mechanisms. *Atmospheric Chemistry and Physics* **2006**, *6*, 4079-4091.
  18. Kuang, C.; McMurry, P. H.; McCormick, A. V.; Eisele, F. L. Dependence of nucleation rates on sulfuric acid vapor concentration in diverse atmospheric

- locations. *Journal of Geophysical Research: Atmospheres* **2008**, *113*, D10209.
19. Riipinen, I.; Sihto, S.; Kulmala, M.; Arnold, F.; Maso, M. D.; Birmili, W.; Saarnio, K.; Teinilä, K.; Kerminen, V.; Laaksonen, A.; Lehtinen, K. E. J. Connections between atmospheric sulphuric acid and new particle formation during QUEST III–IV campaigns in Heidelberg and Hyytiälä. *Atmospheric Chemistry and Physics* **2007**, *7*, 1899-1914.
20. Sipilä, M.; Berndt, T.; Petäjä, T.; Brus, D.; Vanhanen, J.; Stratmann, F.; Patokoski, J.; Mauldin III, R. L.; Hyvärinen, A.; Lihavainen, H.; Kulmala, M. The role of sulfuric acid in atmospheric nucleation. *Science* **2010**, *327*, 1243-1246.
21. Sipilä, M.; Sarnela, N.; Jokinen, T.; Henschel, H.; Junninen, H.; Kontkanen, J.; Richters, S.; Kangasluoma, J.; Franchin, A.; Peräkylä, O.; Rissanen, M. P.; Ehn, M.; Vehkamäki, H.; Kurtén, T.; Berndt, T.; Petäjä, T.; Worsnop, D.; Ceburnis, D.; Kerminen, V.; Kulmala, M.; O'Dowd, C. Molecular-scale evidence of aerosol particle formation via sequential addition of HIO<sub>3</sub>. *Nature* **2016**, *537*, 532-534.
22. Ball, S. M.; Hanson, D. R.; Eisele, F. L.; McMurry, P. H. Laboratory studies of particle nucleation: Initial results for H<sub>2</sub>SO<sub>4</sub>, H<sub>2</sub>O, and NH<sub>3</sub> vapors. *Journal of Geophysical Research: Atmospheres* **1999**, *104*, 23709-23718.
23. Kurtén, T.; Torpo, L.; Ding, C.; Vehkamäki, H.; Sundberg, M. R.; Laasonen, K.; Kulmala, M. A density functional study on water-sulfuric acid-ammonia clusters and implications for atmospheric cluster formation. *Journal of Geophysical Research: Atmospheres* **2007**, *112*, D04210.
24. Torpo, L.; Kurtén, T.; Vehkamäki, H.; Laasonen, K.; Sundberg, M. R.; Kulmala, M. Significance of ammonia in growth of atmospheric nanoclusters. *The Journal of Physical Chemistry A* **2007**, *111*, 10671-10674.
25. Nadykto, A. B.; Yu, F. Strong hydrogen bonding between atmospheric nucleation precursors and common organics. *Chemical Physics Letters* **2007**, *435*, 14-18.
26. Loukonen, V.; Kurtén, T.; Ortega, I. K.; Vehkamäki, H.; Padua, A. A.; Sellegri, K.; Kulmala, M. Enhancing effect of dimethylamine in sulfuric acid nucleation

- in the presence of water – A computational study. *Atmospheric Chemistry and Physics* **2010**, *10*, 4961-4974.
27. DePalma, J. W.; Doren, D. J.; Johnston, M. V. Formation and growth of molecular clusters containing sulfuric acid, water, ammonia, and dimethylamine. *The Journal of Physical Chemistry A* **2014**, *118*, 5464-5473.
28. Boucher, O.; Randal, D.; Artaxo, P.; Bretherton, C.; Feingold, G.; Forster, P.; Kerminen, V.; Kondo, Y.; Liao, H.; Lohmann, U.; Rasch, P.; Satheesh, S. K. Clouds and Aerosols. In *Climate Change 2013: The Physical Science Basis. Contribution of Working Group I to the Fifth Assessment Report of the Intergovernmental Panel on Climate Change*; Stocker, T. F., Qin, D., Plattner, G., Tignor, M., Allen, S. K., Boschung, J., Nauels, A., Xia, Y., Bex, V. and Midgley, P. M., Eds.; Cambridge University Press: Cambridge, United Kingdom and New York, NY, USA, 2013.
29. Almeida, J.; Schobesberger, S.; Kürten, A.; Ortega, I. K.; Kupiainen-Määttä, O.; Praplan, A. P.; Adamov, A.; Amorim, A.; Bianchi, F.; Breitenlechner, M.; David, A.; Dommen, J.; Donahue, N. M.; Downard, A.; Dunne, E.; Duplissy, J.; Ehrhart, S.; Flagan, R. C.; Franchin, A.; Guida, R.; Hakala, J.; Hansel, A.; Heinritzi, M.; Henschel, H.; Jokinen, T.; Junninen, H.; Kajos, M.; Kangasluoma, J.; Keskinen, H.; Kupc, A.; Kurtén, T.; Kvashin, A. N.; Laaksonen, A.; Lehtipalo, K.; Leiminger, M.; Leppä, J.; Loukonen, V.; Makhmutov, V.; Mathot, S.; McGrath, M. J.; Nieminen, T.; Olenius, T.; Onnela, A.; Petäjä, T.; Riccobonoo, F.; Riipinen, I.; Rissanen, M.; Rondo, L.; Ruuskanen, T.; Santos, F. D.; Sarnela, N.; Schallhart, S.; Schnitzhofer, R.; Seinfeld, J. H.; Simon, M.; Sipilä, M.; Stozhkov, Y.; Stratmann, F.; Tomé, A.; Tröstl, J.; Tsagkogeorgas, G.; Vaattovaara, P.; Viisanen, Y.; Virtanen, A.; Vrtala, A.; Wagner, P. E.; Weingartner, E.; Wex, H.; Williamson, C.; Wimmer, D.; Ye, P.; Yli-Juuti, T.; Carslaw, K. S.; Kulmala, M.; Curtius, J.; Baltensperger, U.; Worsnop, D. R.; Vehkamäki, H.; Kirkby, J. Molecular understanding of sulphuric acid–amine particle nucleation in the atmosphere. *Nature* **2013**, *502*, 359-363.
30. Tröstl, J.; Chuang, W. K.; Gordon, H.; Heinritzi, M.; Yan, C.; Molteni, U.; Ahlm, L.; Frege, C.; Bianchi, F.; Wagner, R.; Simon, M.; Lehtipalo, K.; Williamson, C.; Craven, J. S.; Duplissy, J.; Adamov, A.; Almeida, J.; Bernhammer, A.;

- Breitenlechner, M.; Brielke, S.; Dias, A.; Ehrhart, S.; Flagan, R. C.; Franchin, A.; Fuchs, C.; Guida, R.; Gysel, M.; Hansel, A.; Hoyle, C. R.; Jokinen, T.; Junninen, H.; Kangasluoma, J.; Keskinen, H.; Kim, J.; Krapf, M.; Kürten, A.; Laaksonen, A.; Lawler, M.; Leiminger, M.; Mathot, S.; Möhler, O.; Nieminen, T.; Onnela, A.; Petäjä, T.; Piel, F. M.; Miettinen, P.; Rissanen, M. P.; Rondo, L.; Sarnela, N.; Schobesberger, S.; Sengupta, K.; Sipilä, M.; Smith, J. N.; Steiner, G.; Tomè, A.; Virtanen, A.; Wagner, A. C.; Weingartner, E.; Wimmer, D.; Winkler, P. M.; Ye, P.; Carslaw, K. S.; Curtius, J.; Dommen, J.; Kirkby, J.; Kulmala, M.; Riipinen, I.; Worsnop, D. R.; Donahue, N. M.; Baltensperger, U. The role of low-volatility organic compounds in initial particle growth in the atmosphere. *Nature* **2016**, *533*, 527-531.
31. Bey, I.; Aumont, B.; Toupance, G. A modeling study of the nighttime radical chemistry in the lower continental troposphere: 1. Development of a detailed chemical mechanism including nighttime chemistry. *Journal of Geophysical Research: Atmospheres* **2001**, *106*, 9959-9990.
32. Geyer, A.; Alicke, B.; Ackermann, R.; Martinez, M.; Harder, H.; Brune, W.; di Carlo, P.; Williams, E.; Jobson, T.; Hall, S.; Shetter, R.; Stutz, J. Direct observations of daytime NO<sub>3</sub>: Implications for urban boundary layer chemistry. *Journal of Geophysical Research: Atmospheres* **2003**, *108*, 4386.
33. Ayres, B. R.; Allen, H. M.; Draper, D. C.; Brown, S. S.; Wild, R. J.; Jimenez, J. L.; Day, D. A.; Campuzano-Jost, P.; Hu, W.; de Gouw, J.; Koss, A.; Cohen, R. C.; Duffey, K. C.; Romen, P.; Baumann, K.; Edgerton, E.; Takahama, S.; Thornton, J. A.; Lee, B. H.; Lopez-Hilfiker, F. D.; Mohr, C.; Wennberg, P. O.; Nguyen, T. B.; Teng, A.; Goldstein, A. H.; Olson, K.; Fry, J. L. Organic nitrate aerosol formation via NO<sub>3</sub> + biogenic volatile organic compounds in the Southeastern United States. *Atmospheric Chemistry and Physics* **2015**, *15*, 13377-13392.
34. Johnson, D.; Marston, G. The gas-phase ozonolysis of unsaturated volatile organic compounds in the troposphere. *Chemical Society Reviews* **2008**, *37*, 699-716.
35. Wennberg, P. O.; Bates, K. H.; Crouse, J. D.; Dodson, L. G.; McVay, R. C.; Mertens, L. A.; Nguyen, T. B.; Praske, E.; Schwantes, R. H.; Smarte, M. D.; St Clair, J. M.; Teng, A. P.; Zhang, X.; Seinfeld, J. H. Gas-phase reactions

- of isoprene and its major oxidation products. *Chemical Reviews* **2018**, *118*, 3337-3390.
36. Calogirou, A.; Larsen, B. R.; Kotzias, D. Gas-phase terpene oxidation products: A review. *Atmospheric Environment* **1999**, *33*, 1423-1439.
37. Vereecken, L.; Francisco, J. S. Theoretical studies of atmospheric reaction mechanisms in the troposphere. *Chemical Society Reviews* **2012**, *41*, 6259-6293.
38. Atkinson, R. Gas-phase tropospheric chemistry of volatile organic compounds: 1. Alkanes and alkenes. *Journal of Physical and Chemical Reference Data* **1997**, *26*, 215-290.
39. Rissanen, M. P.; Kurtén, T.; Sipilä, M.; Thornton, J. A.; Kangasluoma, J.; Sarnela, N.; Junninen, H.; Jørgensen, S.; Schallhart, S.; Kajos, M. K.; Taipale, R.; Springer, M.; Mentel, T. F.; Ruuskanen, T.; Petäjä, T.; Worsnop, D. R.; Kjaergaard, H. G.; Ehn, M. The formation of highly oxidized multifunctional products in the ozonolysis of cyclohexene. *Journal of the American Chemical Society* **2014**, *136*, 15596-15606.
40. Jørgensen, S.; Knap, H. C.; Otkjær, R. V.; Jensen, A. M.; Kjeldsen, M. L.; Wennberg, P. O.; Kjaergaard, H. G. Rapid hydrogen shift scrambling in hydroperoxy-substituted organic peroxy radicals. *The Journal of Physical Chemistry A* **2016**, *120*, 266-275.
41. Knap, H. C.; Jørgensen, S. Rapid hydrogen shift reactions in acyl peroxy radicals. *The Journal of Physical Chemistry A* **2017**, *121*, 1470-1479.
42. Rissanen, M. P.; Kurtén, T.; Sipilä, M.; Thornton, J. A.; Kausiala, O.; Garmash, O.; Kjaergaard, H. G.; Petäjä, T.; Worsnop, D. R.; Ehn, M.; Kulmala, M. Effects of chemical complexity on the autoxidation mechanisms of endocyclic alkene ozonolysis products: From methylcyclohexenes toward understanding  $\alpha$ -pinene. *The Journal of Physical Chemistry A* **2015**, *119*, 4633-4650.
43. Kurtén, T.; Rissanen, M. P.; Mackeprang, K.; Thornton, J. A.; Hyttinen, N.; Jørgensen, S.; Ehn, M.; Kjaergaard, H. G. Computational study of hydrogen shifts and ring-opening mechanisms in  $\alpha$ -pinene ozonolysis products. *The Journal of Physical Chemistry A* **2015**, *119*, 11366-11375.



44. Peeters, J.; Müller, J.; Stavrou, T.; Nguyen, V. S. Hydroxyl radical recycling in isoprene oxidation driven by hydrogen bonding and hydrogen tunneling: The upgraded LIM1 mechanism. *The Journal of Physical Chemistry A* **2014**, *118*, 8625-8643.
45. Lloyd, A. C.; Atkinson, R.; Lurmann, F. W.; Nitta, B. Modeling potential ozone impacts from natural hydrocarbons—I. Development and testing of a chemical mechanism for the NO<sub>x</sub>-air photooxidations of isoprene and  $\alpha$ -pinene under ambient conditions. *Atmospheric Environment* **1983**, *17*, 1931-1950.
46. Paulot, F.; Crouse, J. D.; Kjaergaard, H. G.; Kürten, A.; Clair, J. M. S.; Seinfeld, J. H.; Wennberg, P. O. Unexpected epoxide formation in the gas-phase photooxidation of isoprene. *Science* **2009**, *325*, 730-733.
47. D'Ambro, E. L.; Møller, K. H.; Lopez-Hilfiker, F. D.; Schobesberger, S.; Liu, J.; Shilling, J. E.; Lee, B. H.; Kjaergaard, H. G.; Thornton, J. A. Isomerization of second-generation isoprene peroxy radicals: Epoxide formation and implications for secondary organic aerosol yields. *Environmental Science & Technology* **2017**, *51*, 4978-4987.
48. Junninen, H.; Ehn, M.; Petäjä, T.; Luosujärvi, L.; Kotiaho, T.; Kostianen, R.; Rohner, U.; Gonin, M.; Fuhrer, K.; Kulmala, M.; Worsnop, D. R. A high-resolution mass spectrometer to measure atmospheric ion composition. *Atmospheric Measurement Techniques* **2010**, *3*, 1039-1053.
49. Yan, C.; Nie, W.; Äijälä, M.; Rissanen, M. P.; Canagaratna, M. R.; Massoli, P.; Junninen, H.; Jokinen, T.; Sarnela, N.; Häme, S. A.; Schobesberger, S.; Canonaco, F.; Yao, L.; Prévôt, S. H.; Petäjä, T.; Kulmala, M.; Sipilä, M.; Worsnop, D. R.; Ehn, M. Source characterization of highly oxidized multifunctional compounds in a boreal forest environment using positive matrix factorization. *Atmospheric Chemistry and Physics* **2016**, *16*, 12715-12731.
50. Jokinen, T.; Sipilä, M.; Junninen, H.; Ehn, M.; Lönn, G.; Hakala, J.; Petäjä, T.; Mauldin Iii, R. L.; Kulmala, M.; Worsnop, D. R. Atmospheric sulphuric acid and neutral cluster measurements using CI-API-TOF. *Atmospheric Chemistry and Physics* **2012**, *12*, 4117-4125.

51. Jokinen, T.; Sipilä, M.; Richters, S.; Kerminen, V.; Paasonen, P.; Stratmann, F.; Worsnop, D.; Kulmala, M.; Ehn, M.; Herrmann, H.; Berndt, T. Rapid autoxidation forms highly oxidized RO<sub>2</sub> radicals in the atmosphere. *Angewandte Chemie International Edition* **2014**, *53*, 14596-14600.
52. Jokinen, T.; Kausiala, O.; Garmash, O.; Peräkylä, O.; Junninen, H.; Schobesberger, S.; Yan, C.; Sipilä, M.; Rissanen, M. P. Production of highly oxidized organic compounds from ozonolysis of β-caryophyllene: Laboratory and field measurements. *Boreal Environment Research* **2016**, *21*, 262-273.
53. St. Clair, J. M.; McCabe, D. C.; Crouse, J. D.; Steiner, U.; Wennberg, P. O. Chemical ionization tandem mass spectrometer for the in situ measurement of methyl hydrogen peroxide. *Review of Scientific Instruments* **2010**, *81*, 094102.
54. Spencer, K. M.; McCabe, D. C.; Crouse, J. D.; Olson, J. R.; Crawford, J. H.; Weinheimer, A. J.; Knapp, D. J.; Montzka, D. D.; Cantrell, C. A.; Hornbrook, R. S.; Mauldin III, R. L.; Wennberg, P. O. Inferring ozone production in an urban atmosphere using measurements of peroxyntic acid. *Atmospheric Chemistry and Physics* **2009**, *9*, 3697-3707.
55. Danilin, M. Y.; Ko, M.; Bevilacqua, R. M.; Lyjak, L. V.; Froidevaux, L.; Santee, M. L.; Zawodny, J. M.; Hoppel, K. W.; Richard, E. C.; Spackman, J. R.; Weinstock, E. M.; Herman, R. L.; McKinney, K. A.; Wennberg, P. O.; Eisele, F. L.; Stimpfle, R. M.; Scott, C. J.; Elkins, J. W.; Bui, T. V. Comparison of ER-2 aircraft and POAM III, MLS, and SAGE II satellite measurements during SOLVE using traditional correlative analysis and trajectory hunting technique. *Journal of Geophysical Research: Atmospheres* **2002**, *107*, 8315.
56. Crouse, J. D.; DeCarlo, P. F.; Blake, D. R.; Emmons, L. K.; Campos, T. L.; Apel, E. C.; Clarke, A. D.; Weinheimer, A. J.; McCabe, D. C.; Yokelson, R. J.; Jimenez, J. L.; Wennberg, P. O. Biomass burning and urban air pollution over the Central Mexican Plateau. *Atmospheric Chemistry and Physics* **2009**, *9*, 4929-4944.
57. Lee, B. H.; Mohr, C.; Lopez-Hilfiker, F. D.; Lutz, A.; Hallquist, M.; Lee, L.; Romer, P.; Cohen, R. C.; Iyer, S.; Kurtén, T.; Hu, W.; Day, D. A.; Campuzano-Jost, P.; Jimenez, J. L.; Xu, L.; Ng, N. L.; Guo, H.; Weber, R.

- J.; Wild, R. J.; Brown, S. S.; Koss, A.; de Gouw, J.; Olson, K.; Goldstein, A. H.; Seco, R.; Kim, S.; McAvey, K.; Shepson, P. B.; Starn, T.; Baumann, K.; Edgerton, E. S.; Liu, J.; Shilling, J. E.; Miller, D. O.; Brune, W.; Schobesberger, S.; D'Ambro, E. L.; Thornton, J. A. Highly functionalized organic nitrates in the Southeast United States: Contribution to secondary organic aerosol and reactive nitrogen budgets. *Proceedings of the National Academy of Sciences* **2016**, *113*, 1516-1521.
58. Lopez-Hilfiker, F. D.; Mohr, C.; D'Ambro, E. L.; Lutz, A.; Riedel, T. P.; Gaston, C. J.; Iyer, S.; Zhang, Z.; Gold, A.; Surratt, J. D.; Lee, B. H.; Kurtén, T.; Hu, W. W.; Jimenez, J.; Hallquist, M.; Thornton, J. A. Molecular composition and volatility of organic aerosol in the Southeastern US: Implications for IEPOX derived SOA. *Environmental Science & Technology* **2016**, *50*, 2200-2209.
59. Lopez-Hilfiker, F. D.; Lee, B. H.; D'Ambro, E. L.; Thornton, J. A. Constraining the sensitivity of iodide adduct chemical ionization mass spectrometry to multifunctional organic molecules using the collision limit and thermodynamic stability of iodide ion adducts. *Atmospheric Measurement Techniques* **2016**, *9*, 1505.
60. Huey, L. G.; Villalta, P. W.; Dunlea, E. J.; Hanson, D. R.; Howard, C. J. Reactions of  $\text{CF}_3\text{O}^-$  with atmospheric trace gases. *The Journal of Physical Chemistry* **1996**, *100*, 190-194.
61. Phillips, G. J.; Pouvesle, N.; Thieser, J.; Schuster, G.; Axinte, R.; Fischer, H.; Williams, J.; Lelieveld, J.; Crowley, J. N. Peroxyacetyl nitrate (PAN) and peroxyacetic acid (PAA) measurements by iodide chemical ionisation mass spectrometry: First analysis of results in the boreal forest and implications for the measurement of PAN fluxes. *Atmospheric Chemistry and Physics* **2013**, *13*, 1129-1139.
62. De Gouw, J. A.; Goldan, P. D.; Warneke, C.; Kuster, W. C.; Roberts, J. M.; Marchewka, M.; Bertman, S. B.; Pszenny, A.; Keene, W. C. Validation of proton transfer reaction-mass spectrometry (PTR-MS) measurements of gas-phase organic compounds in the atmosphere during the New England Air Quality Study (NEAQS) in 2002. *Journal of Geophysical Research: Atmospheres* **2003**, *108*, 4682.

63. Hewitt, C. N.; Hayward, S.; Tani, A. The application of proton transfer reaction-mass spectrometry (PTR-MS) to the monitoring and analysis of volatile organic compounds in the atmosphere. *Journal of Environmental Monitoring* **2003**, *5*, 1-7.
64. Tani, A.; Hayward, S.; Hewitt, C. N. Measurement of monoterpenes and related compounds by proton transfer reaction-mass spectrometry (PTR-MS). *International Journal of Mass Spectrometry* **2003**, *223*, 561-578.
65. de Gouw, J.; Warneke, C. Measurements of volatile organic compounds in the Earth's atmosphere using proton-transfer-reaction mass spectrometry. *Mass Spectrometry Reviews* **2007**, *26*, 223-257.
66. Zheng, J.; Ma, Y.; Chen, M.; Zhang, Q.; Wang, L.; Khalizov, A. F.; Yao, L.; Wang, Z.; Wang, X.; Chen, L. Measurement of atmospheric amines and ammonia using the high resolution time-of-flight chemical ionization mass spectrometry. *Atmospheric Environment* **2015**, *102*, 249-259.
67. Hansel, A.; Scholz, W.; Mentler, B.; Fischer, L.; Berndt, T. Detection of RO<sub>2</sub> radicals and other products from cyclohexene ozonolysis with NH<sub>4</sub><sup>+</sup> and acetate chemical ionization mass spectrometry. *Atmospheric Environment* **2018**, *186*, 248-255.
68. Yatavelli, R. L.; Lopez-Hilfiker, F.; Wargo, J. D.; Kimmel, J. R.; Cubison, M. J.; Bertram, T. H.; Jimenez, J. L.; Gonin, M.; Worsnop, D. R.; Thornton, J. A. A chemical ionization high-resolution time-of-flight mass spectrometer coupled to a micro orifice volatilization impactor (MOVI-HRToF-CIMS) for analysis of gas and particle-phase organic species. *Aerosol Science and Technology* **2012**, *46*, 1313-1327.
69. Berndt, T.; Richters, S.; Kaethner, R.; Voigtländer, J.; Stratmann, F.; Sipilä, M.; Kulmala, M.; Herrmann, H. Gas-phase ozonolysis of cycloalkenes: formation of highly oxidized RO<sub>2</sub> radicals and their reactions with NO, NO<sub>2</sub>, SO<sub>2</sub>, and other RO<sub>2</sub> radicals. *The Journal of Physical Chemistry A* **2015**, *119*, 10336-10348.
70. Richters, S.; Herrmann, H.; Berndt, T. Highly oxidized RO<sub>2</sub> radicals and consecutive products from the ozonolysis of three sesquiterpenes. *Environmental Science & Technology* **2016**, *50*, 2354-2362.

71. Berndt, T.; Herrmann, H.; Sipilä, M.; Kulmala, M. Highly oxidized second-generation products from the gas-phase reaction of OH radicals with isoprene. *The Journal of Physical Chemistry A* **2016**, *120*, 10150-10159.
72. Van Voorhis, T.; Head-Gordon, M. Benchmark variational coupled cluster doubles results. *The Journal of Chemical Physics* **2000**, *113*, 8873-8879.
73. Jensen, F. *Introduction to computational chemistry 2nd edition*; John Wiley & Sons, Ltd: 2007; pp 133-191.
74. Adler, T. B.; Knizia, G.; Werner, H. A simple and efficient CCSD(T)-F12 approximation. *The Journal of Chemical Physics* **2007**, *127*, 221106.
75. Riplinger, C.; Sandhoefer, B.; Hansen, A.; Neese, F. Natural triple excitations in local coupled cluster calculations with pair natural orbitals. *The Journal of Chemical Physics* **2013**, *139*, 134101.
76. Riplinger, C.; Neese, F. An efficient and near linear scaling pair natural orbital based local coupled cluster method. *The Journal of Chemical Physics* **2013**, *138*, 034106.
77. Chai, J.; Head-Gordon, M. Long-range corrected hybrid density functionals with damped atom–atom dispersion corrections. *Physical Chemistry Chemical Physics* **2008**, *10*, 6615-6620.
78. Kendall, R. A.; Dunning Jr, T. H.; Harrison, R. J. Electron affinities of the first-row atoms revisited. Systematic basis sets and wave functions. *The Journal of Chemical Physics* **1992**, *96*, 6796-6806.
79. Lee, C.; Yang, W.; Parr, R. G. Development of the Colle-Salvetti correlation-energy formula into a functional of the electron density. *Physical Review B* **1988**, *37*, 785.
80. Becke, A. D. A new mixing of Hartree–Fock and local density-functional theories. *The Journal of Chemical Physics* **1993**, *98*, 1372-1377.
81. Becke, A. D. Density-functional thermochemistry. III. The role of exact exchange. *The Journal of Chemical Physics* **1993**, *98*, 5648-5652.
82. Weigend, F.; Furche, F.; Ahlrichs, R. Gaussian basis sets of quadruple zeta valence quality for atoms H–Kr. *The Journal of Chemical Physics* **2003**, *119*, 12753-12762.
83. Weigend, F.; Ahlrichs, R. Balanced basis sets of split valence, triple zeta valence and quadruple zeta valence quality for H to Rn: Design and

- assessment of accuracy. *Physical Chemistry Chemical Physics* **2005**, *7*, 3297-3305.
84. Werner, H.; Knizia, G.; Manby, F. R. Explicitly correlated coupled cluster methods with pair-specific geminals. *Molecular Physics* **2011**, *109*, 407-417.
85. Peterson, K. A.; Adler, T. B.; Werner, H. Systematically convergent basis sets for explicitly correlated wavefunctions: The atoms H, He, B–Ne, and Al–Ar. *The Journal of Chemical Physics* **2008**, *128*, 084102.
86. Hill, J. G.; Peterson, K. A. Correlation consistent basis sets for explicitly correlated wavefunctions: valence and core–valence basis sets for Li, Be, Na, and Mg. *Physical Chemistry Chemical Physics* **2010**, *12*, 10460-10468.
87. Hill, J. G.; Peterson, K. A. Correlation consistent basis sets for explicitly correlated wavefunctions: Pseudopotential-based basis sets for the post-d main group elements Ga–Rn. *The Journal of Chemical Physics* **2014**, *141*, 094106.
88. Lane, J. R.; Kjaergaard, H. G. Explicitly correlated intermolecular distances and interaction energies of hydrogen bonded complexes. *The Journal of Chemical Physics* **2009**, *131*, 034307.
89. Spartan'14: Wavefunction, Inc.: Irvine, CA. **2014**.
90. Partanen, L.; Vehkamäki, H.; Hansen, K.; Elm, J.; Henschel, H.; Kurtén, T.; Halonen, R.; Zapadinsky, E. Effect of conformers on free energies of atmospheric complexes. *The Journal of Physical Chemistry A* **2016**, *120*, 8613-8624.
91. Halgren, T. A. Merck molecular force field. I. Basis, form, scope, parameterization, and performance of MMFF94. *Journal of Computational Chemistry* **1996**, *17*, 490-519.
92. Halgren, T. A. Merck molecular force field. II. MMFF94 van der Waals and electrostatic parameters for intermolecular interactions. *Journal of Computational Chemistry* **1996**, *17*, 520-552.
93. Halgren, T. A. Merck molecular force field. III. Molecular geometries and vibrational frequencies for MMFF94. *Journal of Computational Chemistry* **1996**, *17*, 553-586.

94. Halgren, T. A.; Nachbar, R. B. Merck molecular force field. IV. Conformational energies and geometries for MMFF94. *Journal of Computational Chemistry* **1996**, *17*, 587-615.
95. Halgren, T. A. Merck molecular force field. V. Extension of MMFF94 using experimental data, additional computational data, and empirical rules. *Journal of Computational Chemistry* **1996**, *17*, 616-641.
96. McGrath, M. J.; Olenius, T.; Ortega, I. K.; Loukonen, V.; Paasonen, P.; Kurtén, T.; Kulmala, M.; Vehkamäki, H. Atmospheric Cluster Dynamics Code: A flexible method for solution of the birth-death equations. *Atmospheric Chemistry and Physics* **2012**, *12*, 2345-2355.
97. Frisch, M.; Trucks, G. W.; Schlegel, H. B.; Scuseria, G. E.; Robb, M. A.; Cheeseman, J. R.; Scalmani, G.; Barone, V.; Mennucci, B.; Petersson, G. A.; Nakatsuji, H.; Caricato, M.; Li, X.; Hratchian, H. P.; Izmaylov, A. F.; Bloino, J.; Zheng, G.; Sonnenberg, J. L.; Hada, M.; Ehara, M.; Toyota, K.; Hasegawa, J.; Ishida, M.; Nakajima, T.; Honda, Y.; Kitao, O.; Nakai, H.; Vreven, T. Gaussian 09, revision D. 01. **2009**.
98. Su, T.; Chesnavich, W. J. Parametrization of the ion–polar molecule collision rate constant by trajectory calculations. *The Journal of Chemical Physics* **1982**, *76*, 5183-5185.
99. Eckart, C. The penetration of a potential barrier by electrons. *Physical Review* **1930**, *35*, 1303.
100. Andersson, S.; Nyman, G.; Arnaldsson, A.; Manthe, U.; Jónsson, H. Comparison of quantum dynamics and quantum transition state theory estimates of the H + CH<sub>4</sub> reaction rate. *The Journal of Physical Chemistry A* **2009**, *113*, 4468-4478.
101. Wigner, E. P. Calculation of the rate of elementary association reactions. *Journal of Chemical Physics* **1937**, *5*, 720-725.
102. Georgievskii, Y.; Klippenstein, S. J. Long-range transition state theory. *The Journal of Chemical Physics* **2005**, *122*, 194103.
103. Glowacki, D. R.; Liang, C.; Morley, C.; Pilling, M. J.; Robertson, S. H. MESMER: an open-source master equation solver for multi-energy well reactions. *The Journal of Physical Chemistry A* **2012**, *116*, 9545-9560.

104. da Silva, G.; Kirk, B. B.; Lloyd, C.; Trevitt, A. J.; Blanksby, S. J. Concerted HO<sub>2</sub> elimination from  $\alpha$ -aminoalkylperoxyl free radicals: Experimental and theoretical evidence from the gas-phase  $\text{NH}_2^{\bullet} \text{CHCO}_2^- + \text{O}_2$  reaction. *The Journal of Physical Chemistry Letters* **2012**, *3*, 805-811.
105. Kaiser, E. W. Temperature and pressure dependence of the C<sub>2</sub>H<sub>4</sub> yield from the reaction C<sub>2</sub>H<sub>5</sub> + O<sub>2</sub>. *The Journal of Physical Chemistry* **1995**, *99*, 707-711.
106. Neese, F. The ORCA program system. *Wiley Interdisciplinary Reviews: Computational Molecular Science* **2012**, *2*, 73-78.
107. Werner, H.; Knowles, P. J.; Knizia, G.; Manby, F. R.; Schütz, M. Molpro: a general-purpose quantum chemistry program package. *Wiley Interdisciplinary Reviews: Computational Molecular Science* **2012**, *2*, 242-253.
108. MOLPRO, version 2012.1, a package of *ab initio* programs, Werner, H.-J.; Knowles, P. J.; Knizia, G.; Manby, F. R.; Schütz, M.; Celani, P.; Korona, T.; Lindh, R.; Mitrushenkov, A.; Rauhut, G.; Shamasundar, K. R.; Adler, T. B.; Amos, R. D.; Bernhardsson, A.; Berning, A.; Cooper, D. L.; Deegan, M. J. O.; Dobbyn, A. J.; Eckert, F.; Goll, E.; Hampel, C.; Hesselmann, A.; Hetzer, G.; Hrenar, T.; Jansen, G.; Köppl, C.; Liu, Y.; Lloyd, A. W.; Mata, R. A.; May, A. J.; McNicholas, S. J.; Meyer, W.; Mura, M. E.; Nicklaß, A.; O'Neill, D. P.; Palmieri, P.; Peng, D.; Pfüger, K.; Pitzer, R.; Reiher, M.; Shiozaki, T.; Stoll, H.; Stone, A. J.; Tarroni, R.; Thorsteinsson, T.; Wang, M., see <http://www.molpro.net>
109. MOLPRO, version 2015.1, a package of *ab initio* programs, Werner, H.-J.; Knowles, P. J.; Knizia, G.; Manby, F. R.; Schütz, M.; Celani, P.; Györfly, W.; Kats, D.; Korona, T.; Lindh, R.; Mitrushenkov, A.; Rauhut, G.; Shamasundar, K. R.; Adler, T. B.; Amos, R. D.; Bernhardsson, A.; Berning, A.; Cooper, D. L.; Deegan, M. J. O.; Dobbyn, A. J.; Eckert, F.; Goll, E.; Hampel, C.; Hesselmann, A.; Hetzer, G.; Hrenar, T.; Jansen, G.; Köppl, C.; Liu, Y.; Lloyd, A. W.; Mata, R. A.; May, A. J.; McNicholas, S. J.; Meyer, W.; Mura, M. E.; Nicklaß, A.; O'Neill, D. P.; Palmieri, P.; Peng, D.; Pfüger, K.; Pitzer, R.; Reiher, M.; Shiozaki, T.; Stoll, H.; Stone, A. J.; Tarroni, R.; Thorsteinsson, T.; Wang, M., see <http://www.molpro.net>.